ETH Zürich

Master Thesis

Gravitational Wave Polarization from Future Detector Measurements

Author

Adrian Boîtier
ETH Zürich
D-PHYS

Supervisors

Lionel Philippoz
Universität Zürich
Physik-Institut

Prof. Dr. Philippe Jetzer
Universität Zürich
Physik-Institut

Prof. Dr. Gian Michele Graf
ETH Zürich
D-PHYS

August 10, 2018

Abstract

By combining the signals of all near future gravitational wave detectors one might detect the gravitational wave background which would allow us to observe the universe at the Planck time. This could help us to get constraints on cosmological models and may give hints on the nature of quantum gravity. Its polarization content can serve as a test of general relativity. In this master thesis we calculate the sensitivity of combined space and ground-based detectors to polarizations of gravitational waves. We first investigate the sensitivity to a homogeneous gravitational wave background, where we find that one can use the time dependence of the sensitivity of certain detector pairs to distinguish between different modes. We then calculate the Fisher matrix for the case of gravitational waves due to point sources.

Contents

1 Introduction **2**

2 Theory and Methods **4**
2.1 Polarizations of gravitational waves 4
2.2 Combined sensitivity of multiple detectors 6
2.3 Optical read-out noise 7
2.4 Overlap reduction functions $\gamma^M_{I,J}(f)$ 10

3 The Symmetry of the Einstein Telescope (ET) **13**
3.1 ET perturbations 15
3.1.1 Irregular triangle 15
3.1.2 Tilted detector planes 17
3.2 Cross correlation of Earth's future detectors 20
3.3 Scenario: ET in the USA 22

4 DECIGO and Correlation with Earth Detectors **24**
4.1 Time-dependent Sensitivity 25
4.2 B-DECIGO 27

5 Gravitational waves from point-sources **29**
5.1 Determination of Location and Polarizations of Point Sources 31

6 Conclusions **37**

A Delta distribution Approximation **38**

B Fisher matrix entries **44**

C Provisory Pictures **46**

1 Introduction

Gravitational waves (GW) have just recently been measured for the first time by the LIGO collaboration [1]. So far one has seen 5 mergers of very massive black holes and one could simultaneously observe a neutron star merger through gravitational waves and all accessible frequency bands of the electromagnetic spectrum. [2, 3] [1]. The results matched with Einstein's theory of relativity up to measurement precision.
Until now many tests of general relativity have been made (the perihelion precession of Mercury, the geodetic precession and the Lense-Thirring effect by Gravity Probe B [4] or the weak equivalence principle by MICROSCOPE [5] for example) and so far, they all agree with general relativity (GR). Modifications to GR have been constrained by experiments, but there are still some possibilities which cannot be excluded, see Will [6] to get an overview. As we will discuss in the next chapter one could for example modify GR by adding a scalar or a vector field, which only couple to the metric and therefore act as correction to Einsteins theory of gravity. These fields would allow additional polarizations to the two tensor polarizations, plus (+) and cross (×), predicted by GR. The scalar field would create the breathing (b) and the longitudinal (l) and the vector field the x and the y polarizations.
The standard model of cosmology describes the creation of the universe as an exponentially fast expansion of a quantum state. In quantum mechanics, no field or degree of freedom can be zero. If one now expands the universe, the quantum fluctuations of the fields get macroscopic and create a homogeneous and isotropic background where all polarizations are excited equally.
Using the electromagnetic spectrum we can only observe events as far back as the cosmic microwave background (CMB). The neutrinos decouple a bit earlier and would allow us to see further back in time, given we would figure out how to measure low energy particles, which almost never interact. If we could however measure a gravitational wave background (GWB), then we could test cosmological models way further back in time. One expects that the gravitational waves decouple at the Planck time due to the weak coupling of the metric to the other fields. This might allow us to get information about quantum gravity and thus an energy scale which is far out of reach of modern particle colliders.
Since one expects all polarizations to be excited in the GWB, one could check whether the additional polarizations predicted by GR modifications are there and thus get restrictions on alternative theories of gravity.

The second-generation detectors advanced LIGO and advanced VIRGO can detect GWs from binary black holes (BBH) and binary neutron stars (BNS) [2]. A similar detector is being built in Japan (KAGRA) [7] and another advanced LIGO is planned for India (IndIGO) [8]. With the Einstein Telescope (ET) [9], a cluster of three detectors arranged in an equilateral triangle with an arm length of 10 km, one plans to build a third-generation detector in Europe which is supposed to be about 10 times more sensitive.
Space detectors are also on their way. LISA pathfinder was successful [10] and LISA [11] is planned for ESA L3 launch. LISA will revolve around the Sun on Earth orbit. DECIGO was originally planned to consist of 4 clusters distributed in Earth orbit around the Sun, each forming a 1000 km equilateral triangle with three satellites [12, 13]. A recent paper [14] proposes a scaled down version (100 km) B-DECIGO (basic) as a first generation of deci-Hz detectors. It is planned to revolve around Earth on an altitude of 2000 km.

The ground-based detectors of the second generation are not capable of detecting the gravita-

[1] An overview of all detections can be found on the LIGO webpage: `https://www.ligo.caltech.edu/page/detection-companion-papers`

tional wave background on their own and it is unlikely that an improvement of about one order of magnitude would suffice. But if we combine the signals of all the detectors which are built to measure BBH and BNS anyway, then one could enhance the sensitivity by three to four orders of magnitude and thus get more restrictive constraints on the GWB or detect it, if we are lucky.
With its high and low frequency interferometers, ET is designed to measure in a frequency range from 1.5 Hz to 10 kHz. It therefore makes perfect sense to cross correlate its signals with the ones of any second-generation detector or DECIGO. The correlation between ET and DECIGO has the advantage that their noise is very different, since ET is Earth-based and DECIGO is in space and therefore does not have any seismic noise for example. LISA however is designed to measure at frequencies between 10^{-4} Hz and 1 Hz. Since its frequency range does not overlap with the ones of ET and DECIGO, cross correlations with them do not make sense.
The advantage of testing GR by using the gravitational wave background is that it is constant and isotropic. One does not have to extract complicated waveforms in a combination of all the 6 possible polarizations from the strain, which may differ, dependent on what modified theory we use. And due to its isotropy, it does not make any sense to distinguish between plus and cross tensor polarizations, and x and y vector polarizations. We can however still distinguish the three modes (tensor T, vector V and scalar S), which can already tell us whether we have to modify GR and if so, with what fields. In the case of point sources, we can determine the direction from which the GW is coming from and the distinction between the polarizations is well defined. However, this makes the calculation more complicated since we have to deal with 8 degrees of freedom instead of 3.

In section 2 we first give two representative examples of modifications to GR and their consequences on gravitational waves. We summarize the derivation of the signal to noise ratio (SNR) for a polarization mode of a combination of multiple detectors as it was done in Nishizawa et al. [15, 16]. Then we generalize the formula for the power spectral density and the overlap reduction functions for detectors on Earth with 90° opening angle, to arbitrary opening angles. We apply this method to ET in section 3 and find that one cannot distinguish the different modes due to the degeneracy of its signals resulting from ET's symmetry and propose a way around this by slightly breaking its symmetry. We then include more detectors and investigate the impact on the sensitivity if certain detectors would be offline. In section 4 we add DECIGO to our detector collection and investigate how the time dependent sensitivity of a cross correlation between DECIGO and Earth detectors can be used to distinguish the three polarization modes, as an alternative method to the maximum likelihood method on all detector pairs. Finally, we derive the SNR for a single polarization and the direction of the GW in the case of point sources in section 5.

2 Theory and Methods

In this section we introduce the techniques we use to calculate the sensitivities to GW-polarizations of various combinations of detectors. We first give a short overview of gravitational waves, how the additional polarizations arise from two representative modifications of GR and their detection using multiple interferometers and statistical tests. We continue with extracting the signal of a correlation between two detectors. Then we take multiple detector pairs and combine their signals in an optimal way to distinguish the polarizations and enhance the sensitivity.
The sensitivity is dependent on the noise power spectrum of the detector and geometry factors, which in the case of a gravitational wave background are the overlap reduction functions. To calculate the sensitivity for a collection of detectors including ET or DECIGO we need to generalize the formula for the noise power spectral density to arbitrary opening angles and we can simplify the expression for the overlap reduction functions for ground-based detectors which comes in handy, since many of the detectors we consider here are ground based.

2.1 Polarizations of gravitational waves

The linearization of the Einstein field equations leads to a linear wave equation for perturbations in the metric. Since the metric must be symmetric, the degrees of freedom of a 4-dimensional tensor of rank 2 are reduced from 16 to 10. The Einstein equations are invariant under a change of reference frame, while the linearized version is only invariant under an infinitesimal change of coordinates, which reduces the degrees of freedom by 4 to 6. By choosing an orthonormal basis $(\hat{m}, \hat{n}, \hat{\Omega})$, where $\hat{\Omega} \parallel \vec{k}$ is the direction of travel [15], we can write a general solution as:

$$h_{ij}(t,\vec{x}) = \begin{pmatrix} h_{11} & h_{12} & h_{13} \\ h_{12} & h_{22} & h_{23} \\ h_{13} & h_{23} & h_{33} \end{pmatrix} e^{2\pi i f\left(t-\frac{\hat{\Omega}\cdot\vec{x}}{c}\right)} + c.c. = \sum_A h_A(t,\vec{x}) e^A_{ij} e^{2\pi i f\left(t-\frac{\hat{\Omega}\cdot\vec{x}_I}{c}\right)} + c.c., \tag{1}$$

where the e^A are the basis tensors of the polarizations we describe below and h_A is the amplitude of the GW in the polarization A.

Thus, we can have at most 6 polarizations. Since this is a vacuum equation in the case of unmodified GR, the equation is invariant under a gauge transformation on the fields $h_{\mu\nu} \mapsto h'_{\mu\nu} = h_{\mu\nu} - \epsilon_{\mu,\nu} - \epsilon_{\nu,\mu}$ with $\Box\epsilon^\mu = 0$. This further reduces the degrees of freedom to the 2 tensor polarizations. They are purely transversal waves, which enlarge distances in one direction and squeeze space in the orthogonal direction. The basis tensors of the tensor mode are given by:

$$e^+ = \hat{m}\otimes\hat{m} - \hat{n}\otimes\hat{n}, \qquad e^\times = \hat{m}\otimes\hat{n} + \hat{n}\otimes\hat{m}. \tag{2}$$

We will now look at two representative examples of modifications of GR and their consequences on gravitational waves.
Adding a scalar field to the Lagrangian is one possibility to modify GR [6]. A general tensor scalar action is:

$$S[g,\phi] = \frac{1}{16\pi G}\int \left[R - 2g^{\mu\nu}\partial_\mu\phi\partial_\nu\phi - U(\phi)\right]\sqrt{-g}d^4x \tag{3}$$

This leads to the two scalar polarizations called the breathing mode, since it stretches and squeezes space simultaneously in all transversal directions, and the longitudinal mode, which is a purely longitudinal wave. Their basis tensors are given by:

$$e^b = \hat{m}\otimes\hat{m} + \hat{n}\otimes\hat{n}, \qquad e^l = \sqrt{2}\hat{\Omega}\otimes\hat{\Omega}. \tag{4}$$

Another possibility would be, to add a vector field Lagrangian as follows:

$$S[g,V] = \frac{1}{16\pi G}\int \left[(1+\omega V_\mu V^\mu)R - K^{\mu\nu}_{\rho\sigma}\nabla_\mu V^\rho \nabla_\nu V\sigma + \lambda(V_\mu V^\mu + 1)\right]\sqrt{-g}d^4x \tag{5}$$

with

$$K^{\mu\nu}_{\rho\sigma} = c_1 g^{\mu\nu}g_{\rho\sigma} + c_2\delta^\mu_\rho\delta^\nu_\sigma + c_3\delta^\mu_\sigma\delta^\nu_\rho - c_4 V^\mu V^\nu g_{\rho\sigma}, \tag{6}$$

where the c_i are coefficients which would have to be determined by experiments.
This modification generates the two vector polarizations which oscillate in direction of travel and in one orthogonal to it and can be written as:

$$e^x = \hat{m}\otimes\hat{\Omega} + \hat{\Omega}\otimes\hat{m}, \qquad\qquad e^y = \hat{n}\otimes\hat{\Omega} + \hat{\Omega}\otimes\hat{n}. \tag{7}$$

These are 6 independent polarizations and we can therefore express a general solution in terms of them:

$$h_{ij}(t,\vec{x}) = \begin{pmatrix} h_b + h_+ & h_\times & h_x \\ h_\times & h_b - h_+ & h_y \\ h_x & h_y & h_l \end{pmatrix} e^{2\pi i f\left(t - \frac{\hat{\Omega}\cdot\vec{x}}{c}\right)} + c.c. \tag{8}$$

When a gravitational wave stretches or squeezes an arm of a Michelson interferometer, then one can observe a phase shift. This phase shift is larger if the amplitude of the wave is larger and if the detector arms are optimally aligned given an incoming wave with a certain polarization. So the signal in the detector can be written as:

$$h_{ij}(t,\vec{x}) = D^{ij}\sum_A h_A(t,\vec{x})e^A_{ij}e^{2\pi i f\left(t-\frac{\hat{\Omega}\cdot\vec{x}}{c}\right)}. \tag{9}$$

The detector tensor $D = \frac{1}{2}(\hat{u}\otimes\hat{u} - \hat{v}\otimes\hat{v})$ describes the orientations of the interferometer arms $\hat{u}$, $\hat{v}$ and the polarization of the wave can be written as a linear combination of the basis tensors e^A described above. If we contract the two tensors, we get a scalar quantity which is called the angular pattern function which describes the geometric dependence of the signal:

$$F^A \coloneqq D^{ij}e^A_{ij}. \tag{10}$$

So, a GW produces one scalar signal in each detector. Thus, we need to combine at least 6 detectors to distinguish them. In the case of a gravitational background we expect a direction independent signal. Therefore, one can only distinguish between the three modes: tensor, vector and scalar. So, 3 independent signals are enough, but more signals would of course improve the sensitivity.
By using the matched filtering method, one can calculate the signal to noise ratio of a certain signal. Since the ET project has declared a signal to noise ratio of at least 8 as their condition to accept an event as an actual signal, we set the SNR to 8 and calculate the minimal amplitude a gravitational wave needs to have to be recognized as a true signal by a certain collection of detectors and use this as a measure of their combined sensitivity.
The SNR is related to the false alarm rate α and detection rate γ by [17]:

$$SNR \geqslant \sqrt{\frac{2}{n}}\left(\mathrm{erfc}^{-1}(2\alpha) - \mathrm{erfc}^{-1}(2\gamma)\right) \tag{11}$$

Once one has chosen a minimal signal to noise ratio, one has to choose either a false alarm or a detection rate. If we would split our observation time ($T = 1\,\mathrm{yr}$ would be a realistic choice for a GWB observation) into small time intervals of for example 4 s and do statistical tests on them, then

one false alarm in 27 000 yr would be equivalent to a false alarm rate of $\alpha = \frac{4\,\mathrm{s}}{27\,000\,\mathrm{yr}} = 4.8 \cdot 10^{-12}$. This would give us about $n = 7.8 \cdot 10^6$ time splits and result in a detection rate $\gamma \approx 1$ under the assumption of an SNR of 8. The detection rate is related to the false dismissal rate β by $\gamma = 1 - \beta$ which gives us a false dismissal rate of $\beta = 3.3 \cdot 10^{-18}$.

We will now derive an expression for the SNR in terms of the GW signal and the detector noise.

2.2 Combined sensitivity of multiple detectors

The signal of a GW is smaller than the noise. To get rid of the noise one can use two tricks. First, we can multiply the Fourier transform of the signal with a suitable filter function, which turns out to be proportional to the signal, and integrate over all frequencies. This method is called matched filtering. Secondly, we can cross correlate the strains $s_{I,J} = h_{I,J} + n_{I,J}$ of two detectors I and J. Since the noise $n_{I,J}$ of the two detectors is not correlated and is also not correlated to the signal $h_{I,J}$, we can get rid of the noise by taking the expectation of the Fourier transform (FT) of the complex conjugated strain $\tilde{s}_I^*$ of detector I multiplied with the FT of the strain $\tilde{s}_J$ of detector J:

$$\mathbb{E}[\tilde{s}_I^* \tilde{s}_J] = \mathbb{E}[\tilde{h}_I^* \tilde{h}_J] + \underbrace{\mathbb{E}[\tilde{h}_I^* \tilde{n}_J]}_{=0} + \underbrace{\mathbb{E}[\tilde{n}_I^* \tilde{h}_J]}_{=0} + \underbrace{\mathbb{E}[\tilde{n}_I^* \tilde{n}_J]}_{=0}. \tag{12}$$

Nishizawa et al. [15] used the matched filtering method on a cross correlated signal and derived the SNR for a detector pair (I, J).
The energy density parameter Ω_{GW} of the GWB can be written as a sum over all modes M and each mode has two polarizations M_1 and M_2 as discussed above:

$$\Omega_{GW}^M(f) = \sum_M \Omega_{GW}^M = \sum_M \left(\Omega_{GW}^{M_1} + \Omega_{GW}^{M_2}\right) \ , \ M = \begin{pmatrix} M_1 \\ M_2 \end{pmatrix} \in \left\{ T = \begin{pmatrix} + \\ \times \end{pmatrix}, V = \begin{pmatrix} x \\ y \end{pmatrix}, S = \begin{pmatrix} b \\ l \end{pmatrix} \right\}.$$

The power spectral density $S_h^{M_i}$ of the polarization M_i is related to its energy density parameter by:

$$\Omega_{GW}^{M_i}(f) = \frac{2\pi^2}{3H_0^2} f^3 S_h^{M_i}(f). \tag{13}$$

By assuming that only one mode M is excited and using the ansatz $S_h^{M_i}(f) = h_{0,M_i}^2 \delta(f' - f)$, where h_{0,M_i} is the amplitude of the polarization M_i, we get the sensitivity of the detector pair to the specific mode M:

$$\begin{aligned}
(SNR_{IJ}^M)^2 &= \frac{3H_0^2}{10\pi^2} \sqrt{T \int_{-\infty}^{\infty} \frac{(\Omega_{GW}^M(|f'|)\gamma_{IJ}^M(|f'|))^2}{f^6 P_I(|f'|) P_J(|f'|)} df'} \\
&= \frac{1}{5} \sqrt{T \int_{-\infty}^{\infty} \frac{(S_h^M(|f'|)\gamma_{IJ}^M(|f'|))^2}{P_I(|f'|) P_J(|f'|)} df'} \\
&= \frac{T}{5} \frac{(h_{0,M_1}^2 + h_{0,M_2}^2)\gamma_{IJ}^M(f)}{\sqrt{P_I(f) P_J(f)}},
\end{aligned} \tag{14}$$

where H_0 is the Hubble constant, T the observation time, $P_{I,J}$ are the noise power spectral densities of the detectors I and J and γ_{IJ}^M is the overlap reduction function defined by:

$$\begin{aligned}
\gamma_{IJ}^M(f) &\coloneqq \frac{5}{2} \int_{\mathbb{S}^2} (F_I^{M_1} F_J^{M_1} + F_I^{M_2} F_J^{M_2}) e^{\frac{2\pi i f}{c} \hat{\Omega}_0 \cdot \Delta \vec{x}_{IJ}} \frac{d\hat{\Omega}}{4\pi} \\
&= \rho_1^M(\alpha) D_I^{ij} D_{ij}^J + \rho_2^M(\alpha) D_{I,k}^i D_J^{kj} \hat{d}_i \hat{d}_j + \rho_3^M(\alpha) D_I^{ij} D_J^{kl} \hat{d}_i \hat{d}_j \hat{d}_k \hat{d}_l,
\end{aligned} \tag{15}$$

with $\alpha(f) \coloneqq \frac{2\pi f|\Delta\vec{x}_{IJ}|}{c}$ and the ρ_i^M are linear combinations of the zeroth, second and fourth spherical Bessel functions.

We again require $SNR \overset{!}{\geqslant} 8$ for a GW with mode M to be considered a true signal. We can rewrite this to get the minimal amplitude a GW would need to be detected as such:

$$|h_0^M(f)|_{min} = 8\sqrt{\frac{5\sqrt{P_I(f)P_J(f)}}{T|\gamma_{IJ}^M(f)|}}. \tag{16}$$

If we have more than two detectors we can use the maximum likelihood method to distinguish the polarizations. We then get an SNR with which we recognize a mode M as derived by Nishizawa et al. [16]:

$$\begin{aligned}(SNR^M)^2 &= \frac{3H_0^2}{10\pi^2}\sqrt{\int_{-\infty}^{\infty}\frac{(\Omega_{GW}^M(f))^2\det\mathbf{F}(f)}{f^6\mathcal{F}_M(f)}df} \\ &= \frac{1}{5}\sqrt{\int_{-\infty}^{\infty}\frac{S_h^M(f)^2\det\mathbf{F}(f)}{\mathcal{F}_M(f)}df}.\end{aligned} \tag{17}$$

Using the same ansatz as above, we get the minimal amplitude we require to not only detect a GW with mode M but also distinguish its polarization with an SNR of at least 8:

$$|h_0^M|_{min} = 8\sqrt{5}\sqrt[4]{\frac{\mathcal{F}_M}{T_{obs}\det\mathbf{F}}}, \tag{18}$$

where the Fisher matrix $\mathbf{F}$ is obtained by summing over the Fisher matrices of all detector pairs (I, J)

$$F_{MM'}(f) = \sum_{(I,J)}\int_0^{T_{obs}}\frac{\gamma_{IJ}^M(t,f)\gamma_{IJ}^{M'}(t,f)}{P_I(f)P_J(f)}dt \tag{19}$$

and $\mathcal{F}_M$ is the determinant of the minor one gets by removing the M-th row and column.

2.3 Optical read-out noise

The quantum fluctuations of the laser cause a fundamental noise source in each detector which is statistically independent from the other detectors. The fluctuation in the number density of photons arriving at the detector causes a random fluctuation in the measured power and a fluctuation in the light pressure on the mirror which causes the mirror to vibrate randomly. By increasing the laser power, the fluctuation in the number density increase in total but is less compared to the average, which causes the relative fluctuations in the measured laser power to decrease, but the pressure and therefore the fluctuations in the position of the mirror increases. So, one has to balance one effect against another which causes an uncertainty relation similar to the one arising from quantum mechanics.

A Michelson interferometer with a Fabry-Perot cavity catches an additional term dependant on the frequency f of the measured gravitational wave and on a pole frequency f_p which is a characteristic of the cavity. The power recycling C appears as a higher and the detector efficiency η as a lower effective power: $(P_0 \mapsto \eta C P_0)$.

The phase shift of a Fabry-Perot interferometer $\Delta\phi_{FP}$ is related to the one of a Michelson interferometer without cavity $\Delta\phi_{Mich}$ by:

$$|\Delta\phi_{FP}| = \frac{2\mathcal{F}}{\pi} \frac{|\Delta\phi_{Mich}|}{\sqrt{1 + \left(\frac{f}{f_p}\right)^2}}, \tag{20}$$

$$|\Delta\phi_{Mich}| \coloneqq \Delta\phi_u - \Delta\phi_v, \tag{21}$$

where $\mathcal{F}$ is the finesse of the Fabry-Perot cavity, L the arm length of the detector, $\Delta\phi_u$ and $\Delta\phi_v$ are the phase shifts in the arms u and v respectively, and f_p the pole frequency of the cavity is given by:

$$f_p \approx \frac{c}{4\mathcal{F}L}. \tag{22}$$

To calculate the phase shift of a Michelson interferometer with opening angle θ we consider an incoming GW with plus polarization:

$$h^+_{\mu\nu} = h_+ \begin{pmatrix} 0 & 0 & 0 & 0 \\ 0 & 1 & 0 & 0 \\ 0 & 0 & -1 & 0 \\ 0 & 0 & 0 & 0 \end{pmatrix} \cos(\omega_{GW} t). \tag{23}$$

The GW effectively stretches space in x-direction and squeezes it in y-direction, as depicted in Figure 1, by a factor $h_+(t - \frac{L}{c})$, using the approximation $\frac{\omega_{GW} L}{c} << 1$.

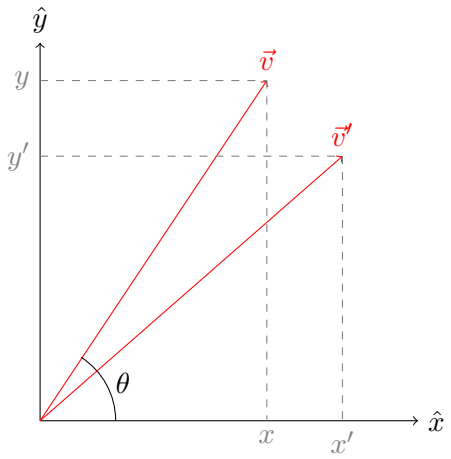

Figure 1: The detector arm $\vec{v}$ of a detector with opening angle θ gets deformed to $\vec{v}'$ under the influence of a gravitational wave with plus polarization. The other detector arm $\vec{u}$ lies on the x-axis.

In this choice of reference frame we can write $\vec{v}$ as:

$$\vec{v} = \begin{pmatrix} x \\ y \end{pmatrix} = L \begin{pmatrix} \cos\theta \\ \sin\theta \end{pmatrix} \quad , \quad |\vec{v}| = L. \tag{24}$$

Making the above approximation, we can write down the components of the deformed arm $\vec{v}'$ and express the change in the coordinates as:

$$x' = \sqrt{x^2 + h_+ x^2} \approx \left[1 + \frac{1}{2} h_+\right] x \quad \Rightarrow \quad \Delta x = \frac{1}{2} h_+ x, \tag{25}$$

$$y' = \sqrt{y^2 - h_+ y^2} \approx \left[1 - \frac{1}{2} h_+\right] y \quad \Rightarrow \quad \Delta y = -\frac{1}{2} h_+ y, \tag{26}$$

where we abbreviated $h_+(t - \frac{L}{c})$ by h_+ and expanded to first order.
The total change in the length of the detector arm is then given by:

$$\begin{aligned}\Delta v &= |\vec{v}'| - |\vec{v}| = \sqrt{x'^2 + y'^2} - \sqrt{x^2 + y^2} \\ &= \frac{1}{2}\frac{2x}{\sqrt{x^2+y^2}}\Delta x + \frac{1}{2}\frac{2y}{\sqrt{x^2+y^2}}\Delta y + \mathcal{O}(\Delta^2) \\ &\approx \frac{\cos\theta L}{L}\Delta x + \frac{\sin\theta L}{L}\Delta y = \frac{1}{2}h_+ L(\cos^2\theta - \sin^2\theta) \end{aligned} \tag{27}$$

Since the light bounces back and forth, the phase shift catches a factor of two: $\Delta\phi_u = 2k_L\Delta u$ and $\Delta\phi_v = 2k_L\Delta v$.

With that we can calculate the amplitude of the Michelson phase shift:

$$\begin{aligned}|\Delta\phi_{Mich}| &= |\Delta\phi_u - \Delta\phi_v| \\ &= \left| k_L h_+ \left(t - \frac{L}{c}\right) L - k_L h_+ \left(t - \frac{L}{c}\right) L(\cos^2\theta - \sin^2\theta) \right| \\ &= \frac{4\pi}{\lambda_L}\sin^2\theta L h_+, \end{aligned} \tag{28}$$

with the wave number k_L and wave length λ_L of the laser: $k_L = \frac{2\pi}{\lambda_L}$.

The change in the pathlength of a photon due to the incoming GW is given by:

$$\Delta L = 2(\Delta u - \Delta v) = \sin^2\theta L h_+ \tag{29}$$

Therefore the transfer function (change in pathlength per GW amplitude) is $\sin^2\theta L$.

By inserting $|\Delta\phi_{Mich}|$ and the transfer function for a general opening angle θ of the detector arms into the equations (9.220), (9.234) and (9.122) of Maggiore [18] and neglecting the efficiency of the photodetector $\eta \approx 1$ we get:

the shot-noise:

$$\sqrt{S_n(f)}\Big|_{shot} = \frac{1}{4\mathcal{F}\sin^2\theta L}\sqrt{\frac{\pi\hbar\lambda_L c}{CP_0}}\sqrt{1 + \left(\frac{f}{f_p}\right)^2}, \tag{30}$$

radiation pressure:

$$\sqrt{S_n(f)}\Big|_{rad} = \frac{16\mathcal{F}}{M\sin^2\theta L}\sqrt{\frac{\hbar C P_0}{\pi\lambda_L c}}\frac{1}{(2\pi f)^2\sqrt{1 + \left(\frac{f}{f_p}\right)^2}} \tag{31}$$

and the optical read-out noise is thus:

$$S_n(f)|_{opt} = S_n(f)|_{shot} + S_n(f)|_{rad}. \tag{32}$$

As an example, we calculate the noise power spectral density due to optical read-out noise for an ET detector. Each ET detector consists of a high- (HF) and a low- (LF) frequency detector which are then used as one to broaden the frequency range. The detector characteristics of these two detectors are listed in Table 1.

	ET-HF	**ET-LF**
Input power (after IMC) P_0	500 W	3 W
Laser wavelength λ_L	1064 nm	1550 nm
Arm length L	10 km	10 km
Mirror mass M	200 kg	211 kg
Finesse $\mathcal{F}$	880	880
Recycling gain C	21.6	21.6

Table 1: Detector characteristics of the high- (HF) and the low- (LF) frequency detectors, taken from the Einstein Telescope proposal [9], section 5.1

We use the following values for the nature constants:
$\hbar = 1.054\,571\,8 \times 10^{-34}\ \frac{\text{kg}\cdot\text{m}^2}{\text{s}}$
$c = 299\,792\,458\ \frac{\text{m}}{\text{s}} \approx 3 \times 10^8\ \frac{\text{m}}{\text{s}}$

With these values and the angle $\alpha = 60°$ we get the sensitivity curves for each detector type in the Einstein Telescope and the resulting sensitivity if ET would be 10 times larger compared to the original one, as shown in Figure 2.

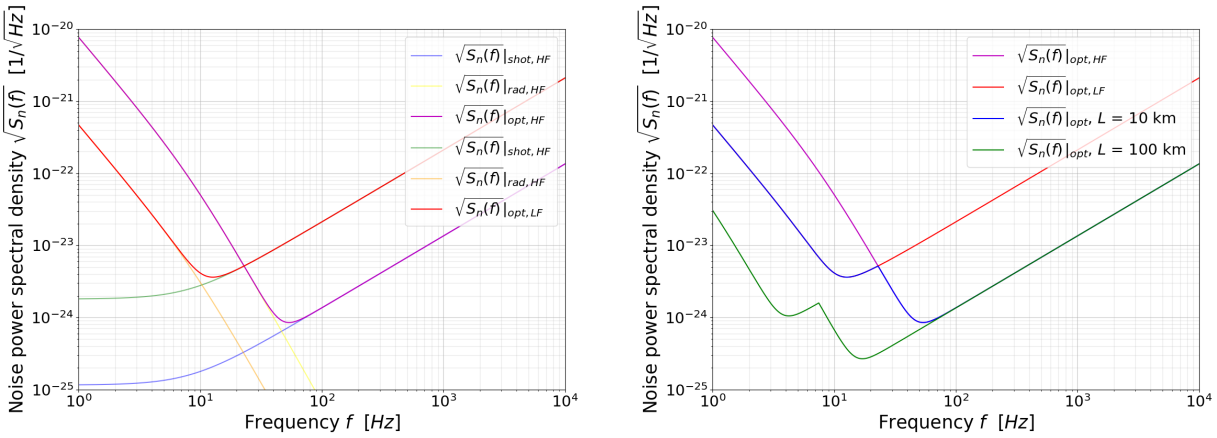

Figure 2: Strain sensitivity due to optical read-out noise (shot and radiation pressure noise) of the Einstein Telescope for the high- (HF) and low-frequency (LF) detector (left) and the comparison of the same detector of length 10 km with length 100 km.

Without either the high- or the low-frequency detector, ET's sensitivity to high or low frequencies would be lower by about an order of magnitude. If one would build ET 10 times larger, it would also be about 10 times more sensitive for frequencies lower than 30 Hz.

2.4 Overlap reduction functions $\gamma^M_{I,J}(f)$

The angular dependence of the pattern functions $F_A(\hat{\Omega})$ can be split into the relative orientation of the detectors towards each other and the orientation of an incoming gravitational wave with respect to the two-detector cluster. The overlap reduction functions account for the relative orientation of the two detectors.
We consider a pair (I, J) of Michelson interferometers on Earth with opening angles ϕ_I and ϕ_J. We denote the direction vectors of the detector arms as $\hat{u}_{I,J}, \hat{v}_{I,J}$ such that $(\hat{u}_{I,J}, \hat{v}_{I,J}, \hat{z}_{I,J})$, with $\hat{z}_{I,J}$ being the direction pointing to the sky, forms a positively oriented frame, as shown in Figure 3.

The relative orientation of the detectors can be described by the angles $\sigma_{I,J}$ between the detector arms $\hat{u}_{I,J}$ and the separation vector $\Delta\vec{x}$, which points from detector I to J.
The direction vectors of the detector arms in the cluster frame are given by:

$$\hat{u}_I = \begin{pmatrix} \cos\sigma_I \\ \sin\sigma_I \\ 0 \end{pmatrix}, \; \hat{v}_I = \begin{pmatrix} \cos(\sigma_I + \phi_I) \\ \sin(\sigma_I + \phi_I) \\ 0 \end{pmatrix}, \; \hat{d} = \frac{1}{\sqrt{2(1-\cos\beta)}} \begin{pmatrix} \sin\beta \\ 0 \\ \cos\beta - 1 \end{pmatrix}$$
$$\hat{u}_J = \begin{pmatrix} \cos\beta\cos\sigma_J \\ \sin\sigma_J \\ -\sin\beta\cos\sigma_J \end{pmatrix}, \; \hat{v}_J = \begin{pmatrix} \cos\beta\cos(\sigma_J + \phi_J) \\ \sin(\sigma_J + \phi_J) \\ -\sin\beta\cos(\sigma_J + \phi_J) \end{pmatrix} \tag{33}$$

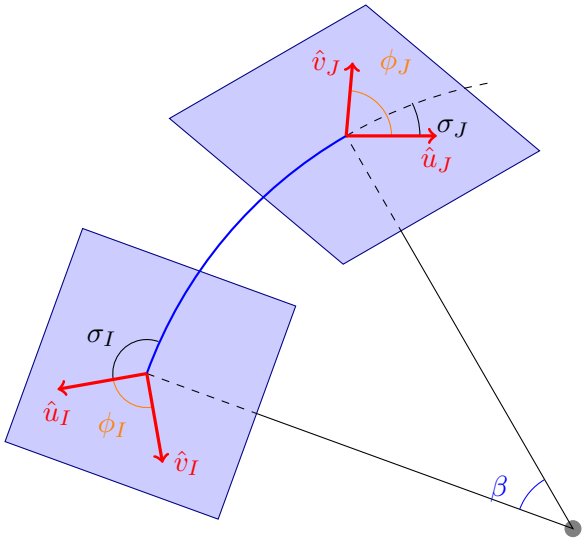

Figure 3: Depiction of the unit vectors of the detector arms $\hat{u}_I, \hat{v}_I, \hat{u}_J, \hat{v}_J$ (red), the opening angles ϕ_I, ϕ_J (orange) and the angles σ_I, σ_J between $\hat{u}_{I,J}$ and the great circle (blue) between the detectors I and J

The contractions of the two detector tensors are then given by:

$$\begin{aligned}
D_I^{ij} D_{ij}^J &= \frac{1}{2}(\hat{u}_I^i \hat{u}_I^j - \hat{v}_I^i \hat{v}_I^j)\frac{1}{2}(\hat{u}_i^J \hat{u}_j^J - \hat{v}_i^J \hat{v}_j^J) \\
&= \frac{1}{4}\left[(\hat{u}_I \cdot \hat{u}_J)^2 - (\hat{v}_I \cdot \hat{u}_J)^2 - (\hat{u}_I \cdot \hat{v}_J)^2 + (\hat{v}_I \cdot \hat{v}_J)^2\right] \\
&= \frac{1}{4}\big[(\sin^2\sigma_I - \sin^2(\sigma_I + \phi_I))(\sin^2\sigma_J - \sin^2(\sigma_I + \phi_J)) \\
&\quad + 2\cos\beta(\sin\sigma_I\cos\sigma_I - \sin(\sigma_I + \phi_I)\cos(\sigma_I + \phi_I)) \\
&\quad\quad \cdot (\sin\sigma_J\cos\sigma_J - \sin(\sigma_J + \phi_J)\cos(\sigma_J + \phi_J)) \\
&\quad + \cos^2\beta(\cos^2\sigma_I - \cos^2(\sigma_I + \phi_I))(\cos^2\sigma_J - \cos^2(\sigma_J + \phi_J))\big] \\
&= \frac{1}{4}\big[(\sin^2\sigma_{1+} - \sin^2\sigma_{1-})(\sin^2\sigma_{2+} - \sin^2\sigma_{2-}) \\
&\quad + \frac{1}{2}\cos\beta(\sin(2\sigma_{1+}) - \sin(2\sigma_{1-}))(\sin(2\sigma_{2+}) - \sin(2\sigma_{2-})) \\
&\quad + \cos^2\beta(\cos^2\sigma_{1+} - \cos^2\sigma_{1-})(\cos^2\sigma_{1+} - \cos^2\sigma_{1-})\big],
\end{aligned} \tag{34}$$

$$
\begin{aligned}
D^i_{I,k} D^{kj}_J \hat{d}_i \hat{d}_j &= \frac{1}{4}\left((\hat{u}_I \cdot \hat{d})\hat{u}_I - (\hat{v}_I \cdot \hat{d})\hat{v}_I\right) \cdot \left((\hat{u}_J \cdot \hat{d})\hat{u}_J - (\hat{v}_J \cdot \hat{d})\hat{v}_J\right) \\
&= \frac{1+\cos\beta}{8}\left[\frac{1}{4}(\sin(2\sigma_{1+}) - \sin(2\sigma_{1-}))(\sin(2\sigma_{2+}) - \sin(2\sigma_{2-}))\right. \\
&\qquad \left. + \cos\beta(\cos^2\sigma_{1+} - \cos^2\sigma_{1-})(\cos^2\sigma_{2+} - \cos^2\sigma_{2-})\right], \qquad (35)
\end{aligned}
$$

$$
\begin{aligned}
D^{ij}_I D^{kl}_J \hat{d}_i \hat{d}_j \hat{d}_k \hat{d}_l &= \frac{1}{4}\left((\hat{u}_I \cdot \hat{d})^2 - (\hat{v}_I \cdot \hat{d})^2\right)\left((\hat{u}_J \cdot \hat{d})^2 - (\hat{v}_J \cdot \hat{d})^2\right) \\
&= \frac{(1+\cos\beta)^2}{16}(\cos^2\sigma_{1+} - \cos^2\sigma_{1-})(\cos^2\sigma_{2+} - \cos^2\sigma_{2-}), \qquad (36)
\end{aligned}
$$

with $\sigma_{1+} \coloneqq \sigma_I + \phi_I$, $\sigma_{1-} \coloneqq \sigma_I$, $\sigma_{2+} \coloneqq \sigma_J + \phi_J$ and $\sigma_{2-} \coloneqq \sigma_J$.

Nishizawa et al. [15] have used a different definition of the angles $\sigma_{1,2}$, which is related to ours by: $\sigma_{1+} = \sigma_1 + \frac{\phi_I}{2}$, $\sigma_{1-} = \sigma_2 - \frac{\phi_I}{2}$, $\sigma_{2+} = \sigma_2 + \frac{\phi_J}{2}$ and $\sigma_{2-} = \sigma_2 - \frac{\phi_J}{2}$.

Finally we get the following expression for the overlap reduction function γ^M_{IJ} of the detectors I and J for the polarization M:

$$
\begin{aligned}
\gamma^M_{IJ}(f) &= \rho^M_1(\alpha) D^{ij}_I D^J_{ij} + \rho^M_2(\alpha) D^i_{I,k} D^{kj}_J \hat{d}_i \hat{d}_j + \rho^M_3(\alpha) D^{ij}_I D^{kl}_J \hat{d}_i \hat{d}_j \hat{d}_k \hat{d}_l \\
&= \frac{1}{16}\left\{4\rho^M_1(\sin^2\sigma_{1+} - \sin^2\sigma_{1-})(\sin^2\sigma_{2+} - \sin^2\sigma_{2-})\right. \\
&\qquad + \left(2\rho^M_1\cos\beta + \rho^M_2\frac{1+\cos\beta}{2}\right) \\
&\qquad \cdot (\sin(2\sigma_{1+}) - \sin(2\sigma_{1-}))(\sin(2\sigma_{2+}) - \sin(2\sigma_{2-})) \\
&\qquad + \left(4\rho^M_1\cos^2\beta + 2\rho^M_2(1+\cos\beta)\cos\beta + \rho^M_3(1+\cos\beta)^2\right) \\
&\qquad \left. \cdot (\cos^2\sigma_{1+} - \cos^2\sigma_{1-})(\cos^2\sigma_{2+} - \cos^2\sigma_{2-})\right\}, \qquad (37)
\end{aligned}
$$

where we defined the argument α and the relation between the arclength β and the distance $|\vec{d}|$ by:

$$
\alpha(f) \coloneqq \frac{2\pi f|\vec{d}|}{c} \ , \ \ |\vec{d}| = 2R_E \sin\frac{\beta}{2}. \qquad (38)
$$

3 The Symmetry of the Einstein Telescope (ET)

We now turn to calculating the sensitivities of various combinations of detectors to figure out how changes could affect the overall sensitivity, which could help us in plans for future detectors. The estimation of the maximal achievable sensitivity could help to find funds for further research if one can show that one can constrain cosmological models and GR modifications significantly.
ET is going to be the largest ground-based detector ever built. It would be of great interest if one could not only detect BBH's and BNS's but also measure the polarizations of the gravitational background. We therefore investigate ET's capability of measuring the GWB polarizations.

Since ET consists of three detectors, one can form three detector pairs which can be used to cross correlate the signal. With the resulting three noise-free signals, one could in principle (as we will see below, for ET those three signals are not independent) solve for the fraction of the power in each polarization mode (tensor T, vector V, scalar S) by using the overlap reduction functions.

The fraction in Eq. (17) can be rewritten as:

$$\begin{aligned}\frac{\det \mathbf{F}}{\mathcal{F}_T} &= \frac{\begin{vmatrix} F_{TT} & F_{TV} & F_{TS} \\ F_{VT} & F_{VV} & F_{VS} \\ F_{ST} & F_{SV} & F_{SS} \end{vmatrix}}{\begin{vmatrix} F_{VV} & F_{VS} \\ F_{SV} & F_{SS} \end{vmatrix}} = \frac{F_{TT}(F_{VV}F_{SS} - F_{SV}F_{VS}) + 2F_{TV}F_{VS}F_{ST} - F_{VV}F_{TS}^2 - F_{SS}F_{VT}^2}{F_{VV}F_{SS} - F_{SV}F_{VS}} \\ &= F_{TT} - \frac{F_{VV}F_{TS}^2 - 2F_{VS}F_{TS}F_{TV} + F_{SS}F_{TV}^2}{F_{VV}F_{SS} - F_{VS}^2}. \end{aligned} \tag{39}$$

This formula was derived via a maximum likelihood method for more than 3 detectors to find 3 modes and is therefore not well defined for 2 detectors, which can be seen by writing out the expression for $\mathcal{F}_T$:

$$\begin{aligned}\mathcal{F}_T &= \sum_{(I,J)} \sum_{(I',J')} \int_0^{T_{obs}} \frac{\gamma_{IJ}^V(t)^2 \gamma_{I'J'}^S(t')^2 - \gamma_{IJ}^V(t)\gamma_{IJ}^S(t)\gamma_{I'J'}^V(t')\gamma_{I'J'}^S(t')}{P_I P_J P_{I'} P_{J'}} dt' dt \\ &= \int_0^{T_{obs}} \frac{\gamma_{IJ}^V(t)^2 \gamma_{IJ}^S(t')^2 - \gamma_{IJ}^V(t)\gamma_{IJ}^S(t)\gamma_{IJ}^V(t')\gamma_{IJ}^S(t')}{P_I^2 P_J^2} dt' dt \quad = 0, \end{aligned} \tag{40}$$

where we used that in our case the overlap reduction functions are time independent: $\gamma_{IJ}^M(t) = \gamma_{IJ}^M(0)$.

Neglecting for the moment factors of $\frac{T_{obs}}{P_I P_J}$, we find:

$$\begin{aligned}\sqrt{F_{VV}F_{SS}} &\sim \sqrt{\sum_{(I,J)} \sum_{(I',J')} (\gamma_{IJ}^V)^2 (\gamma_{I'J'}^S)^2} = \sqrt{(\gamma_{IJ}^V \gamma_{IJ}^S)^2} = \gamma_{IJ}^V \gamma_{IJ}^S \sim F_{VS} \\ \Rightarrow \frac{\det \mathbf{F}}{\mathcal{F}_T} &= F_{TT} - \frac{(\sqrt{F_{VV}}F_{TS} - \sqrt{F_{SS}}F_{TV})^2}{F_{VV}F_{SS} - F_{VS}^2} \\ &= \frac{T_{obs}}{P_I P_J} \left[(\gamma_{IJ}^T)^2 - \frac{(\gamma_{IJ}^V \gamma_{IJ}^T \gamma_{IJ}^S - \gamma_{IJ}^S \gamma_{IJ}^T \gamma_{IJ}^V)^2}{(\gamma_{IJ}^V)^2 (\gamma_{IJ}^S)^2 - (\gamma_{IJ}^V \gamma_{IJ}^S)^2} \right]. \end{aligned} \tag{41}$$

This expression is not well defined since the denominator is zero. In order to see whether the vanishing numerator helps, one has to carefully take the limit of a slightly non-degenerate case, which

we will do below.

Even if one uses the formula for more than 3 detectors, one should be careful with this formula. The fraction is ill defined as soon as the $\sum_{(I,J)} \gamma^M_{I,J}$ commute, which happens for the 3 ET-detectors due to the fact that they are three identical detectors and their symmetric arrangement leads to:

$P_I = P_J =: P \ \ \forall$ Pairs (I, J);

$$\gamma^M_{12} = \gamma^M_{23} = \gamma^M_{31} \quad \forall M \in \{T, V, S\} \quad \Rightarrow \quad F_{MM'} = T_{obs} \frac{\gamma_M \gamma_{M'}}{P^2} \tag{42}$$

$$\Rightarrow \quad \sum_{(I,J)} (\gamma^M_{IJ})^2 \sum_{(I,J)} (\gamma^{M'}_{IJ})^2 = 9(\gamma^M_{IJ})^2 (\gamma^{M'}_{IJ})^2 = (\sum_{(I,J)} \gamma^M_{IJ} \gamma^{M'}_{IJ})^2. \tag{43}$$

To use the formula for the ET-detector we have to break the symmetry by changing the overlap reduction function of one detector pair by a small amount $\epsilon(f)$ and then take the limit:

$$\epsilon(f) \to 0 \quad \forall f.$$

We do this without loss of generality for the example of $M = T$. We perturb one of the overlap reduction functions:

$$\gamma^M_{12} = \gamma^M_{23} = \gamma^M_{31} - \epsilon_M =: \gamma_M \quad \forall M \in \{T, V, S\};$$

When we plug this into the denominator and numerator of the fraction in the right-hand side of Eq. (39) we get:

$$\begin{aligned} \mathcal{F}_T = F_{VV} F_{SS} - F^2_{VS} &= \left(\frac{T_{obs}}{P^2}\right)^2 \left(\sum_{(I,J)} (\gamma^V_{IJ})^2 \sum_{(I,J)} (\gamma^S_{IJ})^2 - (\sum_{(I,J)} \gamma^V_{IJ} \gamma^S_{IJ})^2 \right) \\ &= 2 \left(\frac{T_{obs}}{P^2}\right)^2 (\epsilon_V \gamma_S - \epsilon_S \gamma_V)^2 \end{aligned} \tag{44}$$

and

$$\begin{aligned} F_{VV} F^2_{TS} + F_{SS} F^2_{TV} - 2 F_{TV} F_{VS} F_{TS} = \left(\frac{T_{obs}}{P^2}\right)^3 \big(& 6\gamma^2_T (\gamma^2_S \epsilon^2_V + \gamma^2_V \epsilon^2_S - 2\gamma_V \gamma_S \epsilon_V \epsilon_S) \\ & + \gamma_T (\gamma^2_V \epsilon^2_S + \gamma^2_S \epsilon^2_V - 8\gamma_V \gamma_S \epsilon_V \epsilon_S) \epsilon_T - 3(\gamma_V \gamma^2_S \epsilon_V + \gamma^2_V \gamma_S \epsilon_S) \epsilon^2_T \\ & - 2\gamma_T (\gamma_S \epsilon^2_V \epsilon_S + \gamma_V \epsilon_V \epsilon^2_S) \epsilon_T + 2(\gamma^2_V \epsilon^2_S + \gamma^2_S \epsilon^2_V - 4\gamma_V \gamma_S \epsilon_V \epsilon_S) \epsilon^2_T \\ & - 2\gamma_T \epsilon_T \epsilon^2_V \epsilon^2_S - (\gamma_V \epsilon_V \epsilon^2_S + \gamma_S \epsilon^2_V \epsilon_S) \epsilon^2_T \big). \end{aligned} \tag{45}$$

Plugging this into the full expression of Eq. (39) and taking the limit we arrive at:

$$\begin{aligned}
\frac{\det \mathbf{F}}{\mathcal{F}_T} &= F_{TT} - \frac{F_{VV}F_{TS}^2 - 2F_{VS}F_{TS}F_{TV} + F_{SS}F_{TV}^2}{F_{VV}F_{SS} - F_{VS}^2} \\
&= \frac{T_{obs}}{P^2}(3\gamma_T^2 + 2\gamma_T\epsilon_T + \epsilon_T^2) - \frac{T_{obs}}{P^2}\frac{1}{2(\gamma_V\epsilon_S - \gamma_S\epsilon_V)^2}\big(6\gamma_T^2(\gamma_V\epsilon_S - \gamma_S\epsilon_V)^2 \\
&\quad + \gamma_T(\gamma_V\epsilon_S - \gamma_S\epsilon_V)^2\epsilon_T - 6\gamma_T\gamma_V\gamma_S\epsilon_T\epsilon_V\epsilon_S - 3\gamma_V\gamma_S(\gamma_V\epsilon_S + \gamma_S\epsilon_V)\epsilon_T^2 \\
&\quad - 2\gamma_T(\gamma_V\epsilon_S + \gamma_S\epsilon_V)\epsilon_T\epsilon_V\epsilon_S + 2(\gamma_V\epsilon_S - \gamma_S\epsilon_V)^2\epsilon_T^2 - 4\gamma_V\gamma_S\epsilon_T^2\epsilon_V\epsilon_S \\
&\quad -2\gamma_T\epsilon_T\epsilon_V^2\epsilon_S^2 - (\gamma_V\epsilon_S + \gamma_S\epsilon_V)\epsilon_T^2\epsilon_V\epsilon_S\big) \\
&= \frac{T_{obs}}{P^2}\left(3\gamma_T^2 + 2\gamma_T\epsilon_T + \epsilon_T^2 - 3\gamma_T^2 - \frac{1}{2}\gamma_T\epsilon_T - \epsilon_T^2\right. \\
&\quad + \frac{1}{2}(3\gamma_V\gamma_S\epsilon_T + 2\gamma_T\epsilon_V\epsilon_S + \epsilon_T\epsilon_V\epsilon_S)\epsilon_T\frac{\gamma_V\epsilon_S + \gamma_S\epsilon_V}{(\gamma_V\epsilon_S - \gamma_S\epsilon_V)^2} \\
&\quad \left.+(3\gamma_T\gamma_V\gamma_S + 2\gamma_V\gamma_S\epsilon_T + \gamma_T\epsilon_V\epsilon_S)\frac{\epsilon_T\epsilon_V\epsilon_S}{(\gamma_V\epsilon_S - \gamma_S\epsilon_V)^2}\right) \\
&= \frac{T_{obs}}{P^2}\left(\frac{3}{2}\gamma_T\epsilon_T + \frac{3}{2}\gamma_V\gamma_S\epsilon_T\frac{\epsilon_T(\gamma_V\epsilon_S + \gamma_S\epsilon_V)}{(\gamma_V\epsilon_S - \gamma_S\epsilon_V)^2} + 3\gamma_T\gamma_V\gamma_S\epsilon_T\frac{\epsilon_V\epsilon_S}{(\gamma_V\epsilon_S - \gamma_S\epsilon_V)^2}\right) \\
&\quad + \mathcal{O}(\epsilon^2) \quad \overset{\epsilon\to 0}{\longrightarrow} \quad 0.
\end{aligned} \tag{46}$$

Due to the symmetry of the Einstein Telescope it is impossible to separate the modes out of the signal. The overlap reduction functions of each detector pair are the same, since they only depend on their relative orientation. Therefore, the detector correlation matrix Π has a vanishing determinant and the relation between the cross-correlated signals and the modes of the gravitational wave background cannot be inverted:

$$\det \Pi = \begin{vmatrix} \gamma_{12}^T & \gamma_{12}^V & \gamma_{12}^S \\ \gamma_{23}^T & \gamma_{23}^V & \gamma_{23}^S \\ \gamma_{31}^T & \gamma_{31}^V & \gamma_{31}^S \end{vmatrix} = \begin{vmatrix} \gamma_T & \gamma_V & \gamma_S \\ \gamma_T & \gamma_V & \gamma_S \\ \gamma_T & \gamma_V & \gamma_S \end{vmatrix} = 0. \tag{47}$$

3.1 ET perturbations

We have seen in the previous section that one cannot distinguish between the three polarization modes with the ET detectors although we have three signals, because of the symmetric arrangement of those interferometers.
So, one has to break the symmetry in order to make the three rows in the detector correlation matrix independent. We are going to consider two ways of doing that perturbatively and use the framework of the previous section to determine their impact on the sensitivity, which will allow us to compare both methods.

3.1.1 Irregular triangle

We make one angle smaller by a small angle ϵ_ϕ and make another angle bigger by the same amount, which leaves the third angle unchanged. With that we have a completely irregular triangle with three different angles and therefore the overlap reduction functions of all three detector pairs become different and the detector correlation matrix becomes invertible.

Changing the angles will also change the arm lengths and therefore the distance between a detector pair. We use the sine-law to determine the impact of a change in the angles on the change

in the distance δ.
To estimate the order of magnitude of effect of the perturbation on the detector correlation matrix, we calculate the change in the overlap reduction function of the detector pair $(1,2)$, when we shrink the angle ϕ_3 and enlarge ϕ_1 by ϵ_ϕ, which leaves ϕ_2 unchanged but shortens d_{12}:

$$\frac{d-\delta}{\sin(\phi_3)} = \frac{d}{sin(\phi_1)} \ , \ \ \phi_3 = \phi - \epsilon_\phi \ , \ \ \phi_1 = \phi + \epsilon_\phi \ , \ \ \phi = \frac{\pi}{3}. \tag{48}$$

To first order we get:

$$\delta \approx \sqrt{3} d \epsilon_\phi. \tag{49}$$

With that expression, we can relate the effects of a change in the distance to the change in the angles:

$$\rho_i^M \mapsto (\rho_i^M)^{(0)} - \sqrt{3}\alpha(\rho_i^M)'\epsilon_\phi, \tag{50}$$

$$\cos\beta \mapsto \cos\beta^{(0)} + \sqrt{3}\frac{d^2}{R_E^2}\epsilon_\phi. \tag{51}$$

The only coordinate angle that changes is σ_{1+}. Therefore, we insert the values of the other angles:

$$\sigma_{1-} = 0 \ , \ \ \sigma_{1+} \mapsto \sigma_{1+}^{(0)} + \epsilon_\phi \ , \ \ \sigma_{1+}^{(0)} = \frac{\pi}{3} \ , \ \ \sigma_{2-} = \frac{2\pi}{3} \ , \ \ \sigma_{2+} = \pi; \tag{52}$$

$$\begin{aligned}
\gamma_{12}^M = \frac{1}{16}\Bigg\{ & -3\rho_1^M \sin^2\sigma_{1+} + \frac{\sqrt{3}}{2}\left[2\rho_1^M\cos\beta + \rho_2^M\frac{1+\cos\beta}{2}\right]\sin(2\sigma_{1+}) \\
& + \frac{3}{4}\left[4\rho_1^M\cos^2\beta + 2\rho_2^M(1+\cos\beta)\cos\beta + \rho_3^M(1+\cos\beta)^2\right](\cos^2\sigma_{1+} - 1)\Bigg\} \\
\mapsto \frac{1}{16}\Bigg\{ & -3\left((\rho_1^M)^{(0)} - \sqrt{3}\alpha(\rho_1^M)'\epsilon_\phi\right)\left(\sin^2\sigma_{1+}^{(0)} + 2\sin\sigma_{1+}^{(0)}\cos\sigma_{1+}^{(0)}\epsilon_\phi\right) \\
& + \frac{\sqrt{3}}{2}\Bigg[2\left((\rho_1^M)^{(0)} - \sqrt{3}\alpha(\rho_1^M)'\epsilon_\phi\right)\left(\cos\beta^{(0)} + \sqrt{3}\frac{d^2}{R_E^2}\epsilon_\phi\right) \\
& + \frac{1}{2}\left((\rho_2^M)^{(0)} - \sqrt{3}\alpha(\rho_2^M)'\epsilon_\phi\right)\left(1 + \cos\beta^{(0)} + \sqrt{3}\frac{d^2}{R_E^2}\epsilon_\phi\right)\Bigg]\left(\sin(2\sigma_{1+}^{(0)}) + 2\cos(2\sigma_{1+}^{(0)})\epsilon_\phi\right) \\
& + \frac{3}{4}\Bigg[4\left((\rho_1^M)^{(0)} - \sqrt{3}\alpha(\rho_1^M)'\epsilon_\phi\right)\left(\cos\beta^{(0)} + \sqrt{3}\frac{d^2}{R_E^2}\epsilon_\phi\right)^2 \\
& + 2\left((\rho_2^M)^{(0)} - \sqrt{3}\alpha(\rho_2^M)'\epsilon_\phi\right)\left(1 + \cos\beta^{(0)} + \sqrt{3}\frac{d^2}{R_E^2}\epsilon_\phi\right)\left(\cos\beta^{(0)} + \sqrt{3}\frac{d^2}{R_E^2}\epsilon_\phi\right) \\
& + \left((\rho_3^M)^{(0)} - \sqrt{3}\alpha(\rho_3^M)'\epsilon_\phi\right)\left(1 + \cos\beta^{(0)} + \sqrt{3}\frac{d^2}{R_E^2}\epsilon_\phi\right)^2\Bigg]\left(\cos^2\sigma_{1+}^{(0)} - 2\cos\sigma_{1+}^{(0)}\sin\sigma_{1+}^{(0)}\epsilon_\phi - 1\right)\Bigg\}.
\end{aligned} \tag{53}$$

We can simplify this expression, by plugging in the values for $\sigma_{1+}^{(0)}$ and approximating $\cos\beta^{(0)}$, using that $\frac{d^2}{R_E^2} = 2.5 \cdot 10^{-6} \ll 1$:

$$\cos\beta^{(0)} = 1 - \frac{d^2}{2R_E^2} \approx 1. \tag{54}$$

With that we get to first order in ϵ_ϕ:

$$\begin{aligned}\epsilon_M \approx \frac{1}{16}\Bigg\{&-\frac{3\sqrt{3}}{2}\left[(\rho_1^M)^{(0)}-\frac{3}{2}\alpha(\rho_1^M)'\right]-\frac{\sqrt{3}}{2}\left[2(\rho_1^M)^{(0)}+3\alpha(\rho_1^M)'+(\rho_2^M)^{(0)}+\frac{3}{2}\alpha(\rho_2^M)'\right]\\&-\frac{3\sqrt{3}}{4}\left[2\left((\rho_1^M)^{(0)}+(\rho_2^M)^{(0)}+(\rho_3^M)^{(0)}\right)-3\alpha\left((\rho_1^M)'+(\rho_2^M)'+(\rho_3^M)'\right)\right]\Bigg\}\epsilon_\phi\\ \approx -\frac{\sqrt{3}}{32}\Bigg\{&8(\rho_1^M)^{(0)}+4(\rho_2^M)^{(0)}+3(\rho_3^M)^{(0)}-3\alpha\left(2(\rho_1^M)'+(\rho_2^M)'+\frac{3}{2}(\rho_3^M)'\right)\Bigg\}\epsilon_\phi. \end{aligned} \tag{55}$$

In Figure 4 we plot the response factor, which multiplies to ϵ_ϕ to get the change in the overlap reduction function ϵ_M.

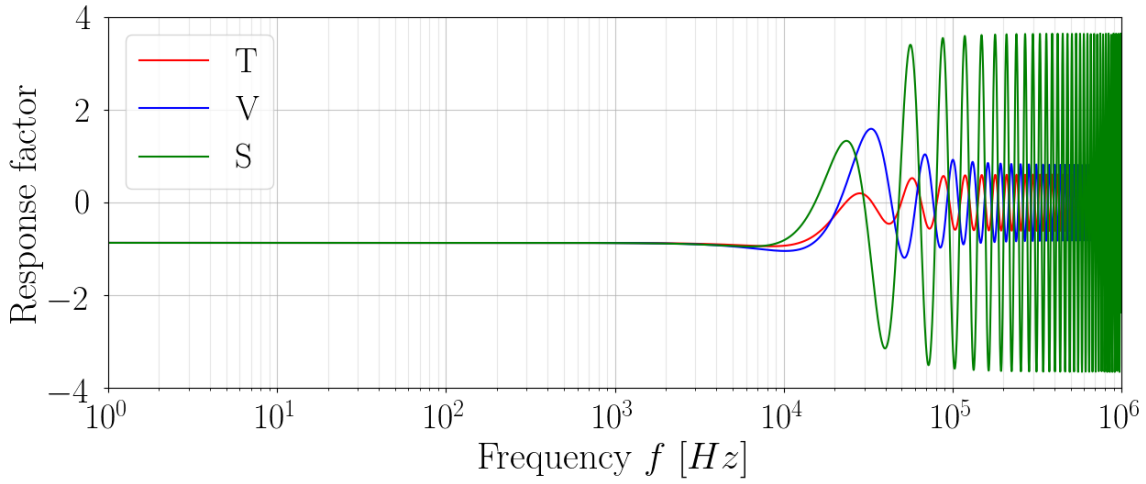

Figure 4: The factor, with which the overlap reduction function responds to a small change in the detector angles.

The response factor stays almost constant at a value of -0.87, since $\alpha \ll 1$ until we get close to the critical frequency $f_{crit} = 3 \times 10^4$ Hz, defined over $\frac{f_{crit} d}{c} \coloneqq 1$.

3.1.2 Tilted detector planes

We leave the angles and the arm-lengths of the three Michelson-interferometers invariant but tilt the plane in which one of the three detectors lies.

We tilt the plane of detector 1, such that $\hat{u}_1$ gets tilted in negative z-direction. The other detector arms stay unchanged ($\hat{u}_J = \hat{u}_J^{(0)}$ for $J \neq 1$ and $\hat{v}_J = \hat{v}_J^{(0)}$ for all J). We can write the perturbation as:

$$\hat{u}_1 \mapsto \hat{u}_1^{(0)} + \delta\hat{u}_1 \ , \quad \delta\hat{u}_1 = \begin{pmatrix} 0 \\ 0 \\ -\delta u \end{pmatrix}. \tag{56}$$

The angle α by which $\hat{u}_1$ is rotated can be approximated by:

$$\alpha \approx \sin\alpha \approx \delta u. \tag{57}$$

We calculate the contractions of the perturbed detector tensors, analogue to (21), (22) and (23) to first order in δu:

$$\begin{aligned} D_1^{ij}D_{ij}^2 &= \frac{1}{4}\left[(\hat{u}_1^{(0)}\cdot\hat{u}_2+\delta\hat{u}_1\cdot\hat{u}_2)^2-(\hat{v}_1\cdot\hat{u}_2)^2-(\hat{u}_1^{(0)}\cdot\hat{v}_2+\delta\hat{u}_1\cdot\hat{v}_2)^2+(\hat{v}_1\cdot\hat{v}_2)^2\right] \\ &\approx \frac{1}{4}(D_1^{ij}D_{ij}^2)^{(0)}+\frac{1}{2}\left[(\hat{u}_1^{(0)}\cdot\hat{u}_2)(\delta\hat{u}_1\cdot\hat{u}_2)-(\hat{u}_1^{(0)}\cdot\hat{v}_2)(\delta\hat{u}_1\cdot\hat{v}_2)\right]. \end{aligned}$$

Using the angles for ET as in Eq. (52) we get:

$$\begin{aligned} \delta(D_1^{ij}D_{ij}^2) &= \frac{1}{2}\left[(\cos\beta\cos\sigma_{1-}\cos\sigma_{2-}+\sin\sigma_{1-}\sin\sigma_{2-})\delta u\sin\beta\cos\sigma_{2-}\right. \\ &\quad \left.-(\cos\beta\cos\sigma_{1-}\cos\sigma_{2+}+\sin\sigma_{1-}\sin\sigma_{2+})\delta u\sin\beta\cos\sigma_{2+}\right] \\ &= \frac{1}{2}\cos\beta\sin\beta(\cos^2\sigma_{2-}-1)\delta u=-\frac{3}{8}\cos\beta\sin\beta\delta u, \end{aligned} \tag{58}$$

$$\begin{aligned} D_{1,k}^iD_2^{kj}\hat{d}_i\hat{d}_j &= \frac{1}{4}\left((\hat{u}_1^{(0)}\cdot\hat{d}+\delta\hat{u}_1\cdot\hat{d})(\hat{u}_1^{(0)}+\delta\hat{u}_1)-(\hat{v}_1\cdot\hat{d})\hat{v}_1\right)\cdot\left((\hat{u}_2\cdot\hat{d})\hat{u}_2-(\hat{v}_2\cdot\hat{d})\hat{v}_2\right) \\ &\approx (D_{1,k}^iD_2^{kj}\hat{d}_i\hat{d}_j)^{(0)}+\frac{1}{4}\left((\delta\hat{u}_1\cdot\hat{d})\hat{u}_1^{(0)}+(\hat{u}_1^{(0)}\cdot\hat{d})\delta\hat{u}_1\right)\cdot\left((\hat{u}_2\cdot\hat{d})\hat{u}_2-(\hat{v}_2\cdot\hat{d})\cdot\hat{v}_2\right), \end{aligned}$$

$$\begin{aligned} \delta(D_{1,k}^iD_2^{kj}\hat{d}_i\hat{d}_j) &= \frac{1}{8(1-\cos\beta)}\left(\delta u(1-\cos\beta)\hat{u}_1^{(0)}+\cos\sigma_{1-}\sin\beta\delta\hat{u}_1\right) \\ &\quad\cdot(\sin\beta\cos\sigma_{2-}\hat{u}_2-\sin\beta\cos\sigma_{2+}\hat{v}_2) \\ &= \frac{\sin\beta}{8}\left(\cos\sigma_{2-}\underbrace{\cos\beta\cos\sigma_{2-}}_{\hat{u}_1^{(0)}\cdot\hat{u}_2}-\underbrace{\cos\beta}_{\hat{u}_1^{(0)}\cdot\hat{v}_2}\right)\delta u+\frac{1+\cos\beta}{8}\left(\cos\sigma_{2-}\underbrace{\delta u\sin\beta\cos\sigma_{2-}}_{\delta\hat{u}_1\cdot\hat{u}_2}-\underbrace{\delta u\sin\beta}_{\delta\hat{u}_1\cdot\hat{v}_2}\right) \\ &= \frac{\sin\beta}{8}\left[\cos\beta(\cos^2\sigma_{2-}-1)+(1+\cos\beta)(\cos^2\sigma_{2-}-1)\right]\delta u \\ &= -\frac{\sin\beta}{8}(1+2\cos\beta)\sin^2\sigma_{2-}\delta u=-\frac{3}{4}\frac{\sin\beta}{8}(1+2\cos\beta)\delta u, \end{aligned} \tag{59}$$

$$\begin{aligned} D_1^{ij}D_2^{kl}\hat{d}_i\hat{d}_j\hat{d}_k\hat{d}_l &= \frac{1}{4}\left((\hat{u}_1^{(0)}\cdot\hat{d}+\delta\hat{u}_1\cdot\hat{d})^2-(\hat{v}_1\cdot\hat{d})^2\right)\left((\hat{u}_2\cdot\hat{d})^2-(\hat{v}_2\cdot\hat{d})^2\right) \\ &= (D_1^{ij}D_2^{kl}\hat{d}_i\hat{d}_j\hat{d}_k\hat{d}_l)^{(0)}+\frac{1}{2}\left((\hat{u}_1^{(0)}\cdot\hat{d})(\delta\hat{u}_1\cdot\hat{d})\right)\left((\hat{u}_2\cdot\hat{d})^2-(\hat{v}_2\cdot\hat{d})^2\right), \end{aligned}$$

$$\begin{aligned} \delta(D_1^{ij}D_2^{kl}\hat{d}_i\hat{d}_j\hat{d}_k\hat{d}_l) &= \frac{1}{8(1-\cos\beta)^2}\cos\sigma_{1-}\sin\beta\delta u(1-\cos\beta)\left(\sin^2\beta\cos^2\sigma_{2-}-\sin^2\beta\cos^2\sigma_{2+}\right) \\ &= \frac{1+\cos\beta}{8}\sin\beta\left(\cos^2\sigma_{2-}-1\right)\delta u=-\frac{3}{4}\frac{1+\cos\beta}{8}\sin\beta\delta u. \end{aligned} \tag{60}$$

Finally, we can patch all terms together, to calculate the perturbation ϵ_M:

$$\begin{aligned} \epsilon_M &= \rho_1^M\delta(D_1^{ij}D_{ij}^2)+\rho_2^M\delta(D_{1,k}^iD_2^{kj}\hat{d}_i\hat{d}_j)+\rho_3^M\delta(D_1^{ij}D_2^{kl}\hat{d}_i\hat{d}_j\hat{d}_k\hat{d}_l) \\ &= -\frac{3}{8}\sin\beta\left\{\rho_1^M\cos\beta+\frac{1}{4}\rho_2^M(1+2\cos\beta)+\frac{1}{4}\rho_3^M(1+\cos\beta)\right\}\delta u. \end{aligned} \tag{61}$$

Again, we find that ϵ_M is almost independent of f, but the effect is three orders of magnitude smaller if we tilt one plane, instead of deforming the equilateral triangle.

$$\epsilon_M = 1.2 \cdot 10^{-3} \delta u \tag{62}$$

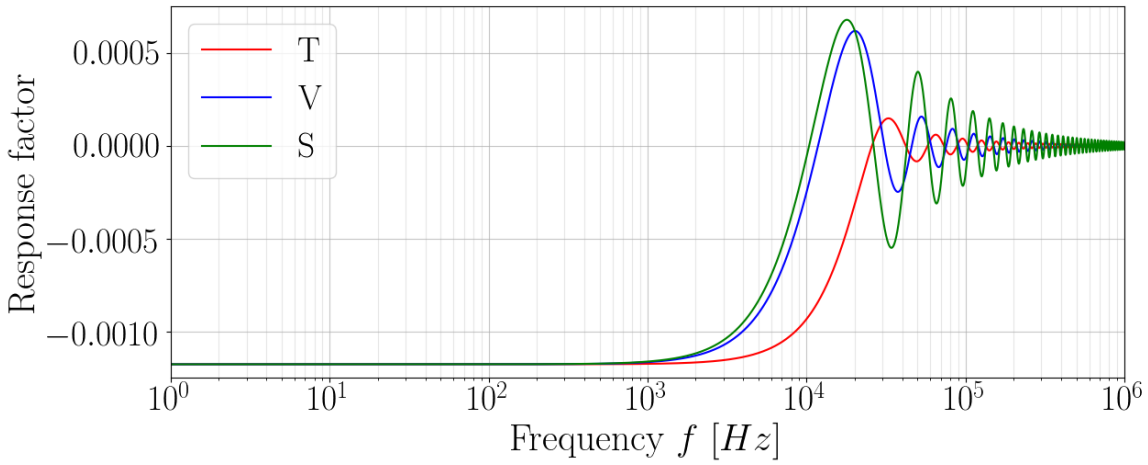

Figure 5: Factor, with which the overlap reduction function responds to a small tilt of one of the detector planes.

The response factor for the tilted plane, shown in Figure 5, stays at about -0.001 for frequencies far below f_{crit} and oscillates ever closer around zero for increasing frequencies above 10^5 Hz. Since ET is designed to measure in a frequency range from 1.5 Hz to 10 kHz the oscillations are not relevant. We find that the response to the same small change in the tilt angle is three orders of magnitude smaller than that of the change in the opening angle.

The effect of a perturbation is at best as small as the angle by which we change ETs geometry, in the case of the irregular triangle. As we will argue in the next section, the problem is resolved if one adds additional detectors, for example LIGO, which exists already anyway, and changing the geometry of ET is therefore not worth the effort.

3.2 Cross correlation of Earth's future detectors

We now turn our attention to combinations of ET with other detectors, which are already existing (LIGO, Virgo) or under construction (KAGRA).
By adding two additional signals to the ET-cluster we break the symmetry and the problem above is resolved. We add the two aLIGO-detectors in Livingston (LL) and Hanford (LH) to our set of detectors, which results in 6 correlation signals out of which 4 (ET-ET, ET-LL, ET-LH, LL-LH) are independent. This allows us to distinguish the polarization modes, even if one of the detectors could not be used for some reason.

To calculate the noise power spectral density of an advanced-LIGO (aLIGO) detector we used the following detector characteristics:
In Figure 6 we plot the combined sensitivity of ET and show the impact on the sensitivity if one of the ET detectors would be offline.
All ET detectors lie in the same plane and are on the scale of Earth at the same place. If one takes out one ET detector the directions in which its detector arms pointed are still covered by the neighbouring detectors. That is why there is no visible change when one of the ET detectors is missing.

Input power (at PRM) P_0	up to 125 W
Laser wavelength λ_L	1064 nm
Arm length L	4 km
Mirror mass M	40 kg
Finesse $\mathcal{F}$	450
Recycling gain C	38

Table 2: Detector characteristics of the aLIGO-detectors, taken from [19], and C from [20]

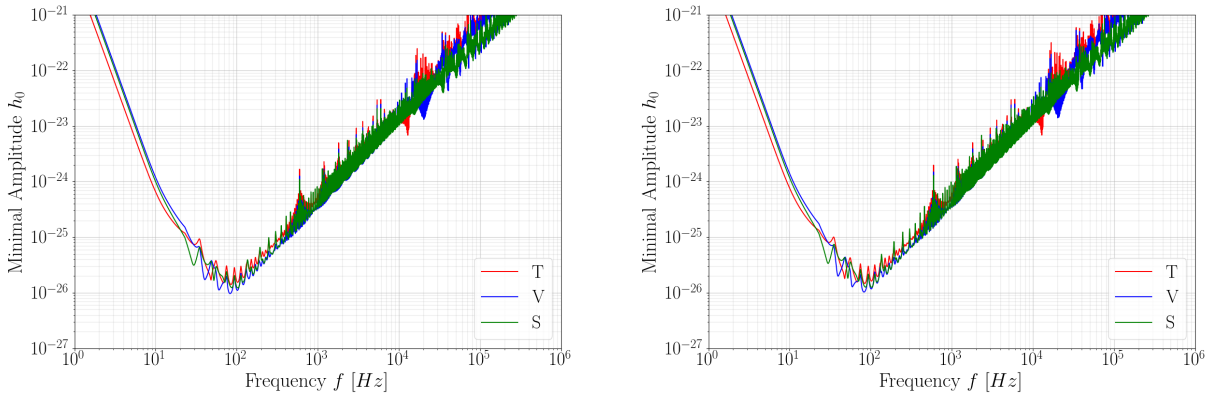

Figure 6: Minimal amplitude necessary to be able to recognize a mode $M \in \{T, V, S\}$ with $SNR = 8$ for a combination of all ET and LIGO detectors (left) and if one of the ET detectors is missing (right).

Since we had 4 independent signals above, distinguishing the modes would still work if we would switch off either the Livingston or the Hanford detector. The resulting sensitivities are shown in Figure 7.

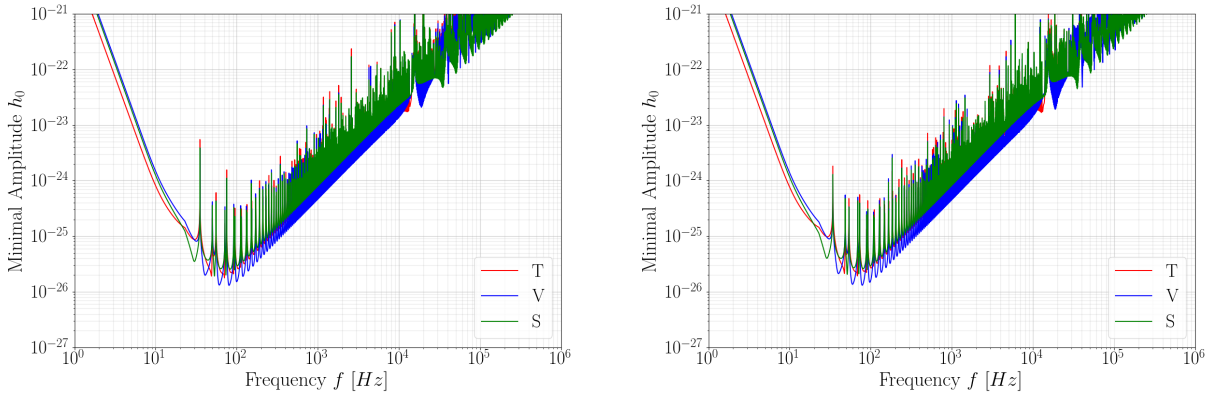

Figure 7: The minimal amplitude sensitivity of the combination of the ET-cluster, with the Livingston detector (left) and with the Hanford detector (right).

If we cross correlate ET with only one LIGO detector, we are less sensitive for the scalar mode above frequencies of 100 Hz. Which LIGO detector we pick does not matter.

Since advanced Virgo and KAGRA will be operating in the future, it only makes sense to add them to our list of detectors and calculate what sensitivity all Earth detectors could reach. In Figure 8 we compare the noise power spectral densities of ET, aLIGO, aVirgo and KAGRA and plot their combined sensitivity.

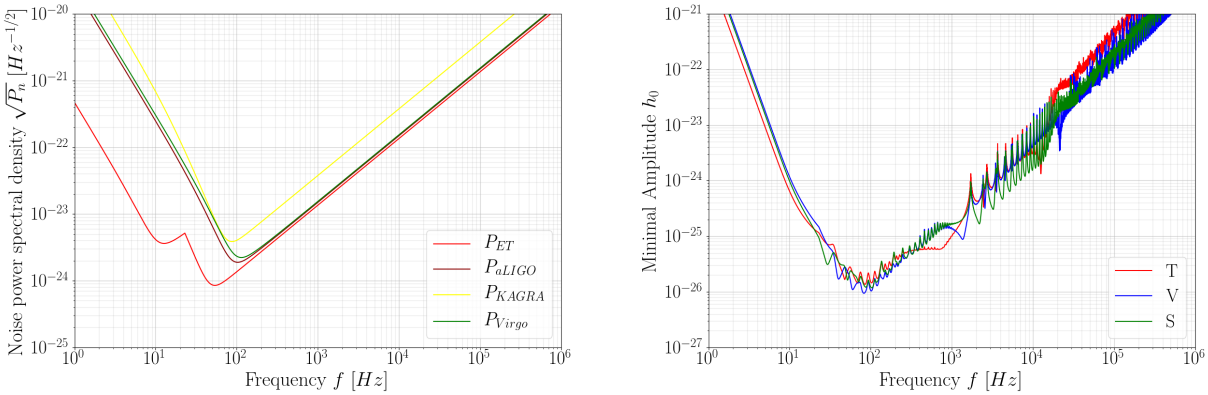

Figure 8: The noise power spectral densities of all involved detectors (left) and the sensitivity of all existing and near future Earth detectors combined (ET, LIGO, Virgo and KAGRA).

When we also add Virgo and KAGRA to the collection we gain sensitivity for frequencies above 100 Hz.

3.3 Scenario: ET in the USA

After the LIGO project one could think of further GW-detectors one could build instead. Another ET-detector in the USA for example would be an option. Maybe one could reuse some of the infrastructure on one of the two LIGO-sites.
In Figure 9 we plot the expected sensitivity of two ET-detectors, one located in Europe and one in the US, either at Livingston or Hanford.

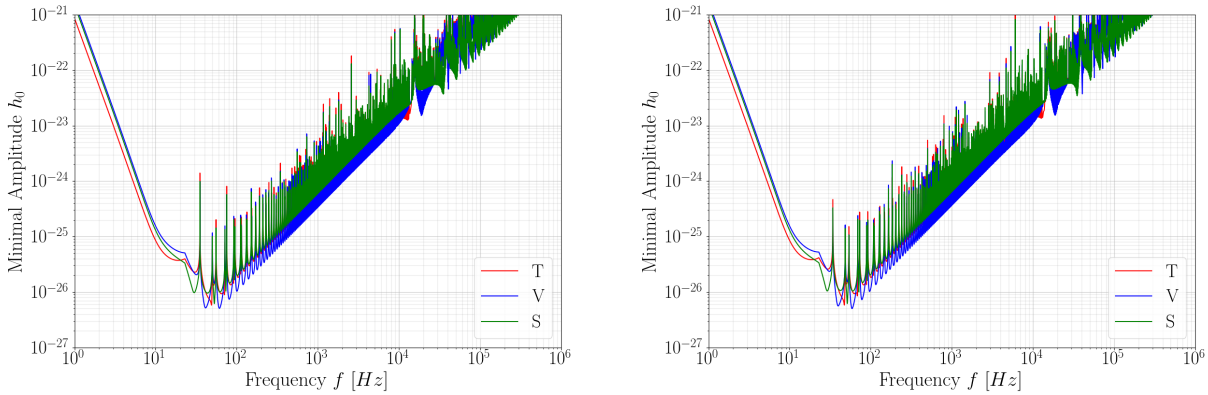

Figure 9: The sensitivity of two ET-detectors. One placed in Europe and the other in Livingston (left) or in Hanford (right).

The cross-correlations between two different ET-Detector clusters deliver enough independent data such that the polarization modes can be separated, and we do not have to worry about the degeneracy of a single cluster. Another effect of the high degree of symmetry in these detector clusters is

that their relative orientations do not matter. The effect of rotating the two detector clusters with respect to each other is on the scale of a factor of about 1.5.
We find that the sensitivity is improved by almost an order of magnitude for frequencies below 100 Hz if we replace the LIGO project by another ET. As before, the choice between Livingston and Hanford makes almost no difference.

4 DECIGO and Correlation with Earth Detectors

After having investigated the combined sensitivity of the detectors on Earth we turn now our attention to space and include projects which may be realized in the farther future. As we mentioned in the introduction we focus on the DECIGO project, since LISA is sensitive in a lower frequency range than the Earth detectors.

DECIGO is a space-based experiment, therefore there is no noise due to vibrations of the ground. Since its sensitive region and the one of ET and LIGO overlap in the frequency range between 10 Hz and 100 Hz, it makes sense to cross correlate their signal to get a higher precision and confidence for the separation of the signal into the three different polarization modes.

The DECIGO experiment consists of four detector clusters. Each cluster is made up by three satellites which form three independent identical Michelson interferometers. One can for example arrange the four clusters in the C3 configuration, presented in [13] and [12], where two clusters are at the same place near Earth and form a star shape and the remaining two form a triangle together with the star-cluster, which has the Sun at its centre. In Figure 10 we compare the noise power spectrum of DECIGO to the ones of ET and LIGO and plot the sensitivity of DECIGO in the C3 configuration.

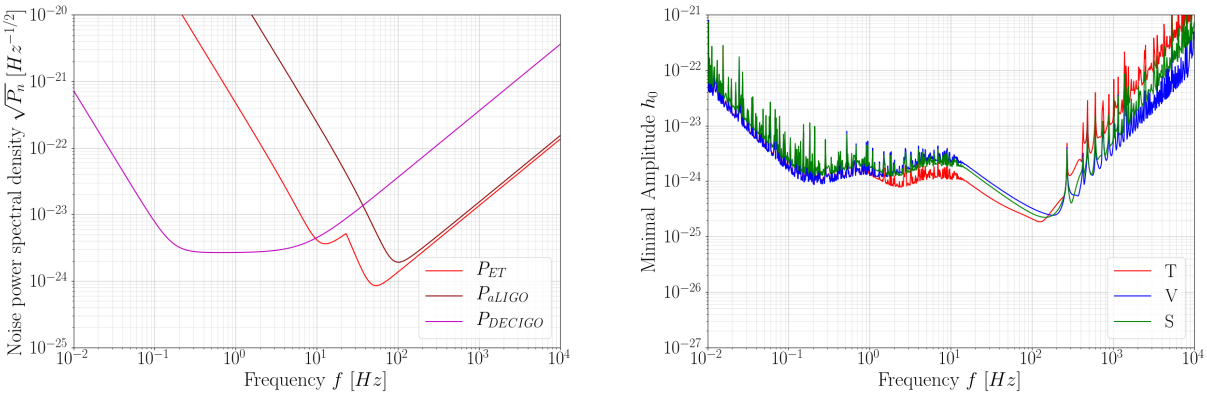

Figure 10: Noise power spectra of a DECIGO, ET and advanced LIGO detector (left) and the sensitivity of DECIGO in C3 configuration.

DECIGO is much more sensitive in the low frequencies than all detectors on Earth combined and is even slightly more sensitive around 100 Hz, which comes in handy when we combine it with Earth detectors.

If we add ET and then LIGO to the set of detectors and sum over all combinations of cross-correlations, we get the plots shown in Figure 11.

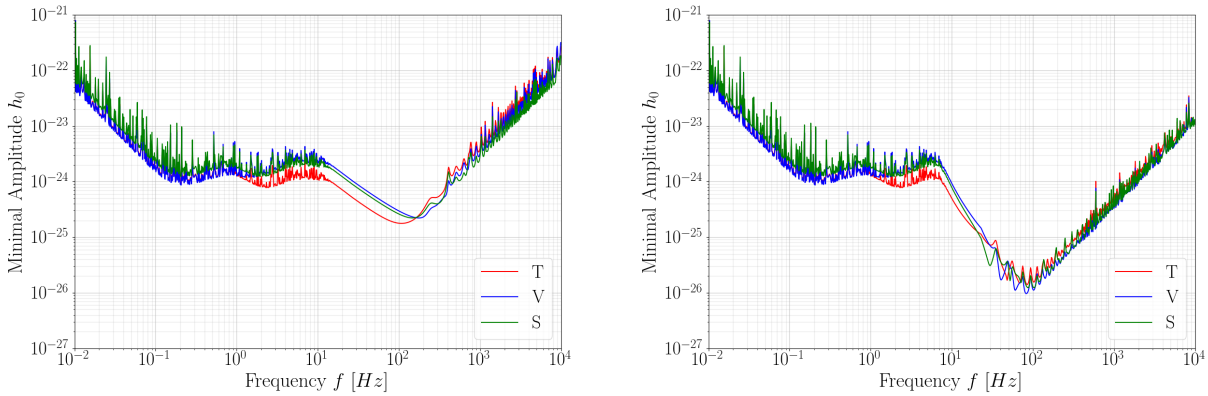

Figure 11: ET and all DECIGO detectors in C3 configuration (left) and together with both LIGO detectors (right), averaged over a total measurement time of one year.

One can see that ET drags the curves down around 10 Hz and mostly above 100 Hz. Especially the tensor and scalar modes are affected. They become about as sensitive as the vector mode. Together with LIGO the sensitivity is enhanced by one order of magnitude at LIGO's most sensitive frequency range around 100 Hz.

4.1 Time-dependent Sensitivity

In the planned DECIGO-configuration C3 we used above, each cluster rotates around its own axis perpendicular to the detector plane as it rotates around the Sun, such that it returns to its original position after a year. A detector on Earth follows Earth rotation and therefore a relatively quick oscillation of one day superposed to a slow oscillation of one year. This combined change in the orientations of the detectors in a DECIGO-cluster relative to detectors on Earth leads to a time varying sensitivity, which is different for each mode, as can be seen in Figure 12. The time dependence of the sensitivity is independent of the frequency. We plot the sensitivities at 10 Hz, where the DECIGO-Earth detector pairs are most sensitive.

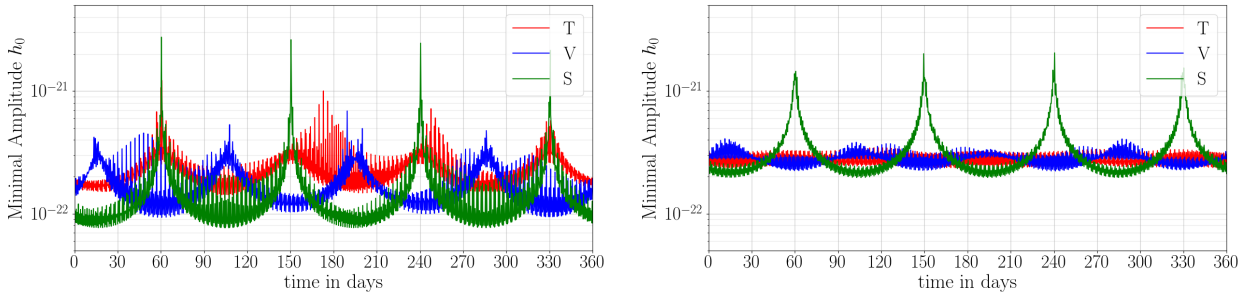

Figure 12: Left: There are two DECIGO detectors in the star cluster, which show the same time dependence when cross correlated with an Earth detector. We take all correlations between those two and all ET and LIGO detectors. Right: In the square configuration (described below) there is one detector in each of the three clusters which are far away from Earth, which have the same time dependence when we correlate them with Earth detectors. We form all pairs of these three with ET and LIGO.

The variation of the sensitivity with time is different if we form the pair with a DECIGO detector close to Earth or one far away from Earth. The location of the peaks is also different for DECIGO-Earth pairs, formed with different DECIGO detectors. Changing the detector on Earth however does not matter, since they are almost at the same place viewed on the solar system scale and oscillate much faster, and therefore do not influence the trend on a monthly scale.
We can now try to optimise the sensitivity by combining all detector pairs with a similar time dependence and average over an integration time of 5 days to not loose to much of the variation. For this we can always form all pairs with the Earth detectors, but we have to be careful which space detectors we pick.

If we want to be able, to clearly separate the vector mode from the other two then it makes sense to pick the C3 configuration, because it has many detectors close to Earth. For two of the detectors in the star cluster the correlation with any Earth detector has almost the same time dependence since their orientation only differs by 30°. In Figure13 we use all those pairs and integrate over 5 days to increase the sensitivity. Due to the fact that the vector modes time dependence is phase-shifted with respect to the other two modes, we can easily separate it from the other two in this case.

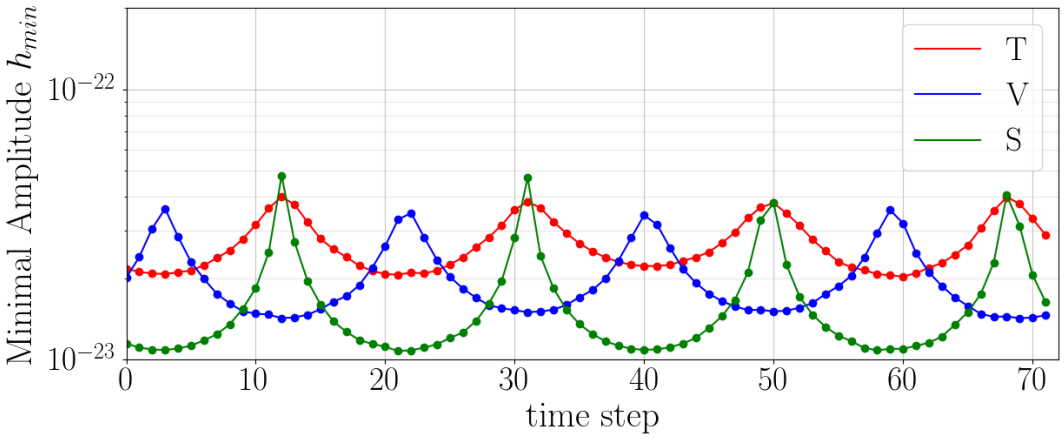

Figure 13: Combined sensitivity of the detector pairs with one of two neighbouring detectors in the star cluster and all ground-based detectors with an integration time of 5 days at a frequency of 10 Hz for one year.

However, if we rather want to identify the scalar mode, then it makes more sense to move more clusters further away from Earth and at best on the opposite side of the orbit around the Sun, because for detectors which are far away from Earth the scalar mode has large peaks which correspond to blind spots. In this case we could arrange the four DECIGO clusters in a square around the Sun, such that only one cluster is close to Earth, and one is on the opposite side of Earth orbit. We can then arrange the initial orientation of the clusters, such that the peaks for one detector of each of the three clusters far from Earth coincide. Their combined time dependent sensitivity is shown in Figure 14.

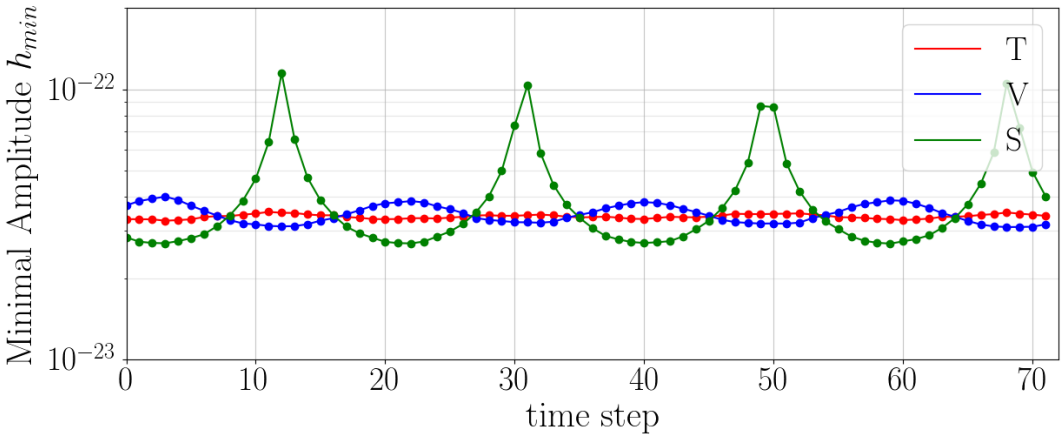

Figure 14: Time dependent sensitivity of detector pairs with one of each of the three clusters far from Earth in the square configuration with all Earth detectors, binned in time with steps of 5 days at a frequency of 10 Hz for one year.

By using the same detectors as above and just combining the data differently, one gets an alternative method to the maximum likelihood method for distinguishing the polarization modes. This can help to check the results and gives a higher confidence on a test of GR, without having to build another experiment.

4.2 B-DECIGO

If we replace DECIGO by the down scaled version B-DECIGO [14], we can see in Figure 15 that we get a somewhat broader region where the sensitivity is better than 10^{-27} but we lose a lot of sensitivity in the lower frequencies, as compared to DECIGO.
B-DECIGO orbits around the Earth on an altitude of 2000 km which is on the same order of magnitude as the radius of the Earth (6371 km). It circles the Earth in a Sun-synchronous dusk-dawn orbit with an angular frequency of about $8.2 \times 10^{-4}\,\mathrm{s}^{-1}$ while Earth rotation corresponds to $7.3 \times 10^{-5}\,\mathrm{s}^{-1}$. This leads to rapidly varying distances and directions of the detector arms and the irrational ratio between the two angular velocities leads to a chaotic behaviour, which makes the use of the time dependent sensitivity very complicated. Additionally one can observe that the sensitivities for the different modes get closer together as one moves a space detector closer to Earth. If one would instead let B-DECIGO take the same type of orbit but on a higher altitude (35 867 km), such that it would circle Earth in one day, one would get almost the same signal every day over a period of about a week, because the change would now be on the time-scale of a year. The detectors would also be far enough from Earth to get relevantly different sensitivity curves for the different modes. The procedure would be more complicated than in the case of DECIGO, but one could still use certain blind spots or other characteristics that only one mode shows. A large disadvantage to DECIGO would also be that one would have to spot those characteristics in a model in advance, since the sensitivities are not periodic.
We compare the time dependent sensitivities of both versions (original B-DECIGO and higher altitude) for time-span of one day in Figure 16.

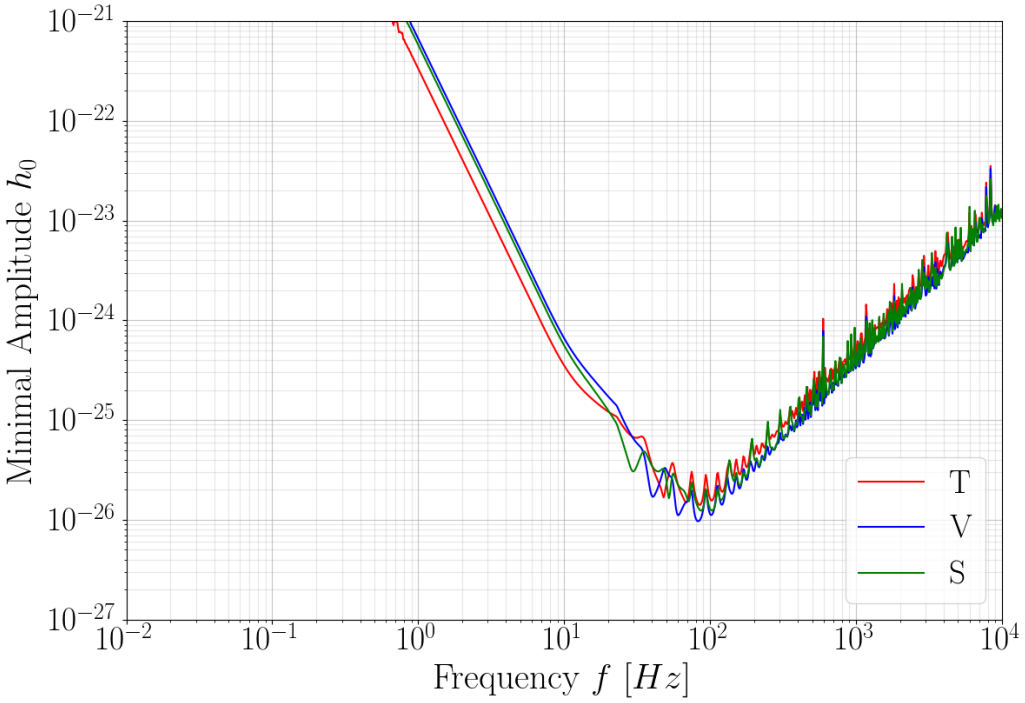

Figure 15: Combined sensitivity of B-DECIGO, ET and both advanced LIGO detectors.

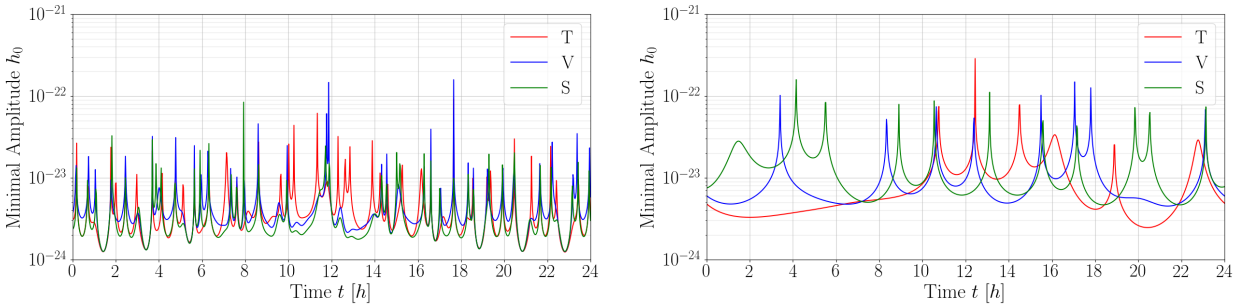

Figure 16: Time dependence of the sensitivity for B-DECIGO for one day (left) and for a higher altitude of 35 867 km (right) for a frequency of 10 Hz.

5 Gravitational waves from point-sources

Until now we have calculated the sensitivity of various combinations of GW-detectors to an isotropic gravitational wave background. Now we attempt to do the same for point sources. Since the signal of a point source is coming from a specific direction, we do not average over all solid angles and our sensitivity becomes direction dependent.
The derivation of the expression for the signal to noise ratio works in analogy to what we have done in section 2 and what was done in Nishizawa et al. [15]. The metric perturbation field at the location of the detector $\vec{x}_I$ can be described as the sum of all gravitational waves, incident on the detector I, coming from all directions:

$$\begin{aligned} h_{ij}(t,\vec{x}_I) &= \sum_A \int_{\mathbb{S}^2} h_A(t,\vec{x}_I,\hat{\Omega}) e^A_{ij}(\hat{\Omega}) d\hat{\Omega} \\ &= \sum_A \int\int_{\mathbb{S}^2} \tilde{h}_A(f,\hat{\Omega}) e^{2\pi i f\left(t-\frac{\hat{\Omega}\cdot\vec{x}_I}{c}\right)} e^A_{ij}(\hat{\Omega}) d\hat{\Omega} df. \end{aligned} \tag{63}$$

For a gravitational wave coming from a point source located at $\hat{\Omega}_0$ in the sky, the frequency-space amplitude takes the form:

$$\tilde{h}_A(f,\hat{\Omega}) = \hat{h}_A(f)\delta(\hat{\Omega}-\hat{\Omega}_0). \tag{64}$$

The response of the detector I to an incoming gravitational wave is described by the so called pattern functions F^A_I, which are defined by contracting the basis tensors e^A of the metric perturbations due to GW's for the polarizations $A \in \{+,\times,x,y,b,l\}$ with the detector tensor D_I:

$$F^A_I(\hat{\Omega}) \coloneqq e^A_{ij}(\hat{\Omega}) D^{ij}_I. \tag{65}$$

Therefore, the Fourier transform of the signal is given by:

$$\tilde{h}_I(f) = \sum_A \tilde{h}_A(f) e^{-2\pi i f \frac{\hat{\Omega}_0\cdot\vec{x}_I}{c}} F^A_I(\hat{\Omega}_0). \tag{66}$$

By cross correlating two strains of different detectors (s_I, s_J) we get rid of the noise as seen in Eq. (12). Thus, the expectation of the Fourier transform of the two strains is:

$$\mathbb{E}[\tilde{h}^*_I(f)\tilde{h}_J(f')] = \tilde{h}^*_A(f)\tilde{h}_{A'}(f') e^{-\frac{2\pi i}{c}\hat{\Omega}_0\cdot(f\vec{x}_I - f'\vec{x}_J)} F^A_I(\hat{\Omega}_0) F^{A'}_J(\hat{\Omega}_0). \tag{67}$$

To maximize the signal to noise ratio, we filter this cross correlated strain with a filter function $\tilde{Q}$:

$$\begin{aligned} \mu \coloneqq \mathbb{E}[Y] &= \int \delta_T(f-f')\mathbb{E}[\tilde{h}^*_I(f)\tilde{h}_J(f')]\tilde{Q}(f') df' df \\ &= \int \tilde{h}^*_A(f)\tilde{h}_{A'}(f) e^{-\frac{2\pi i f}{c}\hat{\Omega}_0\cdot(\vec{x}_I-\vec{x}_J)} F^A_I(\hat{\Omega}_0) F^{A'}_J(\hat{\Omega}_0)\tilde{Q}(f) df, \end{aligned} \tag{68}$$

where Y is the cross correlated signal:

$$Y \coloneqq \int_{-\infty}^{\infty}\int_{-\infty}^{\infty} \delta_T(f-f')\tilde{s}^*_I(f)\tilde{s}_J(f')\tilde{Q}(f-f') df' df. \tag{69}$$

To find the optimal filter function $\tilde{Q}$ we define a scalar product on the space of smooth complex valued functions $C^\infty(\mathbb{C})$:

$$(A,B) \coloneqq \int A^*(f)B(f)P_I(|f|)P_J(|f|) df. \tag{70}$$

Since the noise power spectra diverge algebraically at the origin and at infinity, we have to restrict our functions A and B to the Schwartz-space $\mathcal{S}(\mathbb{C})$.

We can express the expectation of the correlated signal and its variance in terms of this scalar product:

$$\mu = \left(\tilde{Q}, \frac{\tilde{h}_A^* \tilde{h}_{A'} e^{-\frac{2\pi i f}{c}\hat{\Omega}_0 \cdot \Delta\vec{x}} F_I^A F_J^{A'}}{P_I P_J}\right), \tag{71}$$

$$\sigma^2 \coloneqq \mathbb{V}[Y] = \mathbb{E}[Y^2] - \mathbb{E}[Y]^2 \approx \mathbb{E}[Y^2] = \frac{T}{4}(\tilde{Q}, \tilde{Q}), \tag{72}$$

where $\Delta\vec{x} \coloneqq \vec{x}_I - \vec{x}_J$ is the distance vector between the detectors I and J.
The signal to noise ratio is therefore given by:

$$SNR = \frac{\mu}{\sigma} = \frac{\left(\tilde{Q}, \frac{\tilde{h}_A^* \tilde{h}_{A'} e^{-\frac{2\pi i f}{c}\hat{\Omega}_0 \cdot \Delta\vec{x}} F_I^A F_J^{A'}}{P_I P_J}\right)}{\sqrt{\frac{T}{4}(\tilde{Q}, \tilde{Q})}}. \tag{73}$$

This can be maximized, by choosing the filter function $\tilde{Q}$ parallell to the correlated signal with respect to our scalar product.

$$\tilde{Q} \propto \frac{\tilde{h}_A^* \tilde{h}_{A'} e^{-\frac{2\pi i f}{c}\hat{\Omega}_0 \cdot \Delta\vec{x}} F_I^A F_J^{A'}}{P_I P_J} =: \langle h_I h_J \rangle. \tag{74}$$

With a proportionality constant K we get:

$$SNR = \sqrt{\frac{4}{T}} \frac{(K\langle h_I h_J\rangle, \langle h_I h_J\rangle)}{\sqrt{(K\langle h_I h_J\rangle, K\langle h_I h_J\rangle)}} = 2\sqrt{T(\langle h_I h_J\rangle, \langle h_I h_J\rangle)}. \tag{75}$$

Without loss of generality we can therefore choose $\tilde{Q} = \langle h_I h_J \rangle$. Finally, we can calculate the maximal possible signal to noise ratio, with this choice of optimal filter function.

$$\begin{aligned} SNR &= 2\sqrt{\frac{1}{T}(\tilde{Q}, \tilde{Q})} \\ &= 2\sqrt{\frac{1}{T}\int \frac{(\tilde{h}_A^* \tilde{h}_{A'} F_I^A F_J^{A'})^2 e^{\frac{2\pi i f}{c}\hat{\Omega}_0 \cdot \Delta\vec{x}} e^{-\frac{2\pi i f}{c}\hat{\Omega}_0 \cdot \Delta\vec{x}}}{(P_I P_J)^2} P_I P_J df} \\ &= 2\sqrt{\frac{1}{T}\int \frac{(\tilde{h}_A(f)\tilde{h}_{A'}(f) F_I^A(\hat{\Omega}_0) F_J^{A'}(\hat{\Omega}_0))^2}{P_I(|f|)P_J(|f|)} df}. \end{aligned} \tag{76}$$

To extract the frequency dependence and the polarization we insert a harmonic wave with amplitude h_0, frequency f and polarization A.

$$\tilde{h}(f) \stackrel{!}{=} h_0 \delta_T(f - f_0)\delta_{A'A}; \tag{77}$$

$$SNR = 2\sqrt{T^2 \frac{(|h_0|^2 F_I^A(\hat{\Omega}_0) F_J^A \hat{\Omega}_0)^2}{P_I(|f|)P_J(|f|)}} = 2T\frac{|h_0|^2 F_I^A(\hat{\Omega}_0) F_J^A(\hat{\Omega}_0)}{\sqrt{P_I(|f|)P_J(|f|)}}. \tag{78}$$

So, we get the minimal amplitude required to detect a gravitational wave with polarization A and at an SNR of at least 8.

$$|h_0^A(f)|_{min} = \sqrt{32}\frac{\sqrt[4]{P_I(|f|)P_J(|f|)}}{\sqrt{T F_I^A(\hat{\Omega}_0) F_J^A(\hat{\Omega}_0)}} \tag{79}$$

5.1 Determination of Location and Polarizations of Point Sources

If one has more than 8 detector pairs (I, J) (DECIGO would do for example), one can solve for the direction $\hat{\Omega} \simeq (\theta, \phi)$ and all 6 possible polarizations $A \in \{+, \times, x, y, b, l\}$ of an incoming gravitational wave from a point source. We determine the SNR for each quantity under the assumption that the maximum likelihood method is used to calculate them from the at least 8 cross-correlated signals μ_{IJ}. The derivation is analogue to the one given in Nishizawa et al. [16].

The true parameters are denoted by $\vec{\theta}_{true} = (Y, s_A, \hat{\omega})$.

$$Y_{IJ}(f) = T^{\frac{3}{2}} \left| \sum_A \tilde{s}_A(f) F_I^A(\hat{\omega}) \sum_{A'} \tilde{s}_{A'}(f) F_J^{A'}(\hat{\omega}) \right|. \tag{80}$$

The estimated values are $\mu = \langle Y \rangle, h_A = \langle s_A \rangle, \hat{\Omega} = \langle \hat{\omega} \rangle$.

$$\mu_{IJ}(f) = Y_{IJ}(f) + n_{IJ}(f) = T^{\frac{3}{2}} \left| \sum_A \tilde{h}_A(f) F_I^A(\hat{\Omega}) \sum_{A'} \tilde{h}_{A'}(f) F_J^{A'}(\hat{\Omega}) \right|, \tag{81}$$

where the noise $n_{IJ}(f)$ satisfies:

$$\mathbb{E}[n_{IJ}(f)] = 0 \ , \ \mathbb{V}[n_{IJ}(f)] = \frac{T}{4} P_I(f) P_J(f) =: \mathcal{N}_{IJ}(f) \tag{82}$$

Our likelihood function is given by:

$$L(\mu_{IJ}|\vec{\theta}) = \exp\left[- \sum_{(I,J)} \frac{(Y_{IJ} - \mu_{IJ})^2}{2\mathcal{N}_{IJ}} \right]. \tag{83}$$

With the parameters $\vec{\theta} = (\theta, \phi, +, \times, x, y, b, l)$.
The Fisher information matrix can then be calculated as follows:

$$F_{ij} = \mathbb{E}\left[\left(\partial_{\theta_i} \ln L(\mu_{IJ}|\vec{\theta}) \right) \left(\partial_{\theta_j} \ln L(\mu_{IJ}|\vec{\theta}) \right) \right], \tag{84}$$

$$\mathbf{F} = \begin{pmatrix} F_{\theta\theta} & F_{\theta\phi} & F_{\theta A'} \\ F_{\phi\theta} & F_{\phi\phi} & F_{\phi A'} \\ F_{A\theta} & F_{A\phi} & F_{AA'} \end{pmatrix}. \tag{85}$$

To simplify the notation, we define: $\alpha' \coloneqq \frac{2\pi f}{c}$.
We calculate the $\theta\theta$- and the θA-component for a GW with polarization A_0:

$$\begin{aligned} F_{\theta\theta}|_{h=h_{A_0}} &= \mathbb{E}\left[(\partial_\theta \ln L)^2 \right] \Big|_{h=h_{A_0}} = \mathbb{E}\left[\left(\sum_{(I,J)} \frac{1}{\mathcal{N}_{IJ}} (Y_{IJ} - \mu_{IJ}) T^3 |\tilde{h}_{A_0}|^2 \partial_\theta F_I^{A_0} F_J^{A_0} \right)^2 \right] \\ &= \sum_{(I,J)} \frac{1}{\mathcal{N}_{IJ}^2} \underbrace{\mathbb{E}\left[(Y_{IJ} - \mu_{IJ})^2 \right]}_{=\mathcal{N}_{IJ}} T^3 \left(|\tilde{h}_{A_0}|^2 \partial_\theta F_I^{A_0} F_J^{A_0} \right)^2 \\ &\quad + \sum_{(I,J) \neq (I',J')} \frac{1}{\mathcal{N}_{IJ} \mathcal{N}_{I'J'}} \underbrace{\mathbb{E}\left[(Y_{IJ} - \mu_{IJ})(Y_{I'J'} - \mu_{I'J'}) \right]}_{=0} T^3 \left(|\tilde{h}_{A_0}|^2 \partial_\theta F_I^{A_0} F_J^{A_0} \right) \left(|\tilde{h}_{A_0}|^2 \partial_\theta F_{I'}^{A_0} F_{J'}^{A_0} \right) \\ &= \sum_{(I,J)} \frac{T^3}{\mathcal{N}_{IJ}} \left(|\tilde{h}_{A_0}|^2 \partial_\theta F_I^{A_0} F_J^{A_0} \right)^2, \end{aligned} \tag{86}$$

$$
\begin{aligned}
F_{\theta A}|_{h=h_{A_0}} &= \mathbb{E}\left[(\partial_\theta \ln L)\left(\partial_{|\tilde{h}_A|^2} \ln L\right)\right]\Big|_{h=h_{A_0}} \\
&= \mathbb{E}\left[\left(\sum_{(I,J)} \frac{1}{\mathcal{N}_{IJ}}(Y_{IJ}-\mu_{IJ})T^{\frac{3}{2}}|\tilde{h}_{A_0}|^2\partial_\theta F_I^{A_0}F_J^{A_0}\right)\left(\sum_{(I,J)} \frac{1}{\mathcal{N}_{IJ}}(Y_{IJ}-\mu_{IJ})T^{\frac{3}{2}}\partial_{|h_A|^2}|\tilde{h}_I\tilde{h}_J|\right)\right|_{h=h_{A_0}}\Bigg] \\
&= \sum_{(I,J)} \frac{T^3}{\mathcal{N}_{IJ}}\left(F_I^A F_J^A + (1-\delta_{AA_0})\frac{1}{2}\left[\frac{(F_I^A)^2F_J^{A_0}}{F_I^{A_0}} + \frac{(F_J^A)^2F_I A_0}{F_J^{A_0}}\right]\right)|\tilde{h}_{A_0}|^2\partial_\theta F_I^{A_0}F_J^{A_0}. \qquad (87)
\end{aligned}
$$

A detailed calculation of the matrix elements for the more general case, where we have different integration times for different detectors, can be found in Appendix B. We list here the rest of the components again for an A_0 polarization wave:

$$
\begin{aligned}
F_{\phi\phi} &= \sum_{(I,J)} \frac{T^3}{\mathcal{N}_{IJ}}\left(|\tilde{h}_{A_0}|^2\partial_\phi F_I^{A_0}F_J^{A_0}\right)^2, \\
F_{\theta\phi} &= \sum_{(I,J)} \frac{T^3}{\mathcal{N}_{IJ}}(|\tilde{h}_{A_0}|^2)^2\left(\partial_\theta F_I^{A_0}F_J^{A_0}\right)\left(\partial_\phi F_I^{A_0}F_J^{A_0}\right), \\
F_{\phi A} &= \sum_{(I,J)} \frac{T^3}{\mathcal{N}_{IJ}}\left(F_I^A F_J^A + (1-\delta_{AA_0})\frac{1}{2}\left[\frac{(F_I^A)^2F_J^{A_0}}{F_I^{A_0}} + \frac{(F_J^A)^2F_I^{A_0}}{F_J^{A_0}}\right]\right)|\tilde{h}_{A_0}|^2\partial_\phi F_I^{A_0}F_J^{A_0}, \\
F_{AA'} &= \sum_{(I,J)} \frac{T^3}{\mathcal{N}_{IJ}}\left(F_I^A F_J^A + (1-\delta_{AA_0})\frac{1}{2}\left[\frac{(F_I^A)^2F_J^{A_0}}{F_I^{A_0}} + \frac{(F_J^A)^2F_I^{A_0}}{F_J^{A_0}}\right]\right) \\
&\qquad \cdot\left(F_I^{A'}F_J^{A'} + (1-\delta_{A'A_0})\frac{1}{2}\left[\frac{(F_I^{A'})^2F_J^{A_0}}{F_I^{A_0}} + \frac{(F_J^{A'})^2F_I^{A_0}}{F_J^{A_0}}\right]\right). \qquad (88)
\end{aligned}
$$

The inverse of the Fisher matrix is the covariance matrix, which has the variance of θ_i in the i-th diagonal entry. So, the square of the SNR for measuring polarization A is given by:

$$
SNR_A^2 \coloneqq \frac{(|\tilde{h}_A|^2)^2}{\sigma_A^2}\Big|_{h=h_A} = \frac{(|\tilde{h}_A|^2)^2}{(\mathbf{F}^{-1})_{AA}}\Big|_{h=h_A} = \frac{(|\tilde{h}_A|^2)^2\det\mathbf{F}}{\mathcal{F}_A}\Big|_{h=h_A}, \qquad (89)
$$

where $\mathcal{F}_{\theta_i}$ is the determinant of the minor one gets from removing the i-th row and column from the Fisher matrix $\mathbf{F}$.
The SNR of the cross correlation is related to the one of amplitude by:

$$
SNR[\mu] = SNR[h^2] = SNR^2[h]. \qquad (90)
$$

Again, demanding an $SNR[h]$ of at least 8 gives us the minimal amplitude. We can read off the prefactors by comparing with the result for one detector pair above:

$$
|\tilde{h}_A|_{min} = \sqrt{\frac{32}{T}}\sqrt[4]{\left|\frac{\mathcal{F}_A}{\det\mathbf{F}}\right|_{h=h_A}}. \qquad (91)
$$

The variance of the position in the sky is given by:

$$
\mathbb{V}[\theta] = (\mathbf{F}^{-1})_{\theta\theta} = \frac{\mathcal{F}_\theta}{\det\mathbf{F}}, \qquad \mathbb{V}[\phi] = (\mathbf{F}^{-1})_{\phi\phi} = \frac{\mathcal{F}_\phi}{\det\mathbf{F}}. \qquad (92)
$$

It turns out, that the angular pattern functions of the breathing and the longitudinal modes are proportional to each other: $F_I^l = -\sqrt{2}F_I^b$.
Therefore it is impossible to distinguish these two. So, we focus on the distinction between the 4 tensor and vector polarizations and the scalar mode. From now on we use the polarization A as:

$$A \in \{+, \times, x, y, S\}. \tag{93}$$

Realizing the entire DECIGO-project is enormously expensive and therefore questionable whether that is ever going to happen. We therefore do our calculations just for the one DECIGO cluster close to earth ($\phi = -20°$ from Earths position on Earth orbit around the sun), which is the cheapest version and add a plot for the Basic-DECIGO which is supposed to serve as a concept test and will be realized sooner than DECIGO. We keep including ET, which as a ground-based detector is cheaper than DECIGO, and the already existing LIGO detectors.

We use the HEALPix pixelization scheme, to evenly distribute n points on the sky and then average over the h_{min} values for each f and obtain the frequency dependant behaviour of the combined average sensitivity of ET, LIGO and DECIGO in Figure 17.

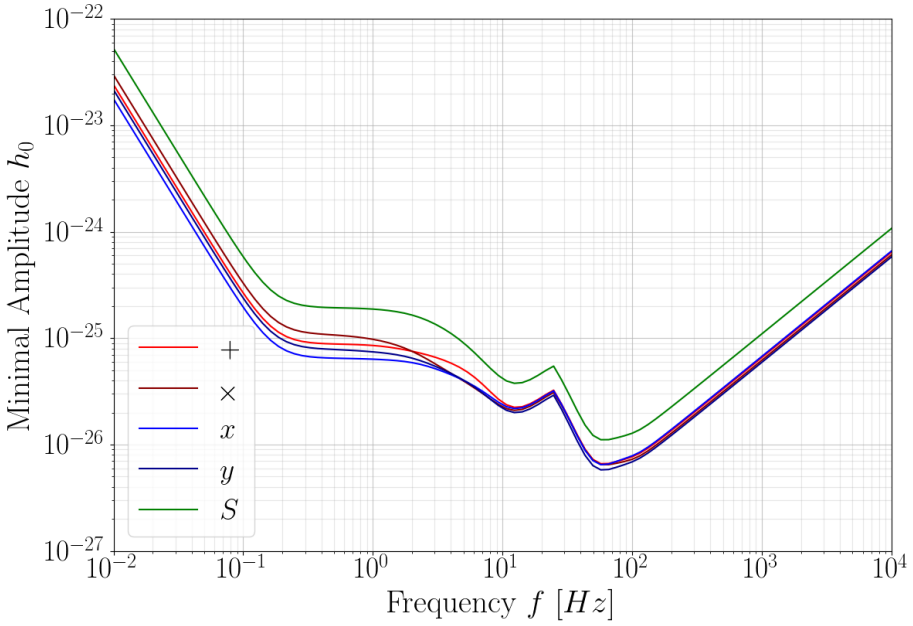

Figure 17: Frequency dependent sensitivity of ET, LIGO and DECIGO towards the polarizations $A \in \{+, \times, x, y, S\}$.

There are two aspects of the frequency dependent standard deviation of θ and ϕ. One is, that if one measures a signal with a certain amplitude, then we can measure the position of the source preciser, if it emits waves in frequencies in which we are more sensitive. We plot this in Figure 18, above for an amlitude $h = 10^{-25}$. As expected, the curves take the shape of the $h(f)$ curve in Figure 17 and have unreasonable values (on the scale of π or even larger than 2π) for frequencies where 10^{-25} is below h_{min}. We cannot even measure those signals, so we should not expect, that we can locate these sources.
The other aspect is, that the standard deviations vary with the frequency, relative to the sensitivity at that frequency. This means, that if we for example take a wave which has twice the minimal

amplitude for each frequency, we still get a frequency dependence. In Figure 18, below we take $h = 2|h_S|_{min}(f)$ because it is always higher than the other polarizations and we can therefore detect it, no matter which polarization we choose and for any fixed frequency we have the same amplitude for all polarizations. This allows us to compare the polarizations with each other.

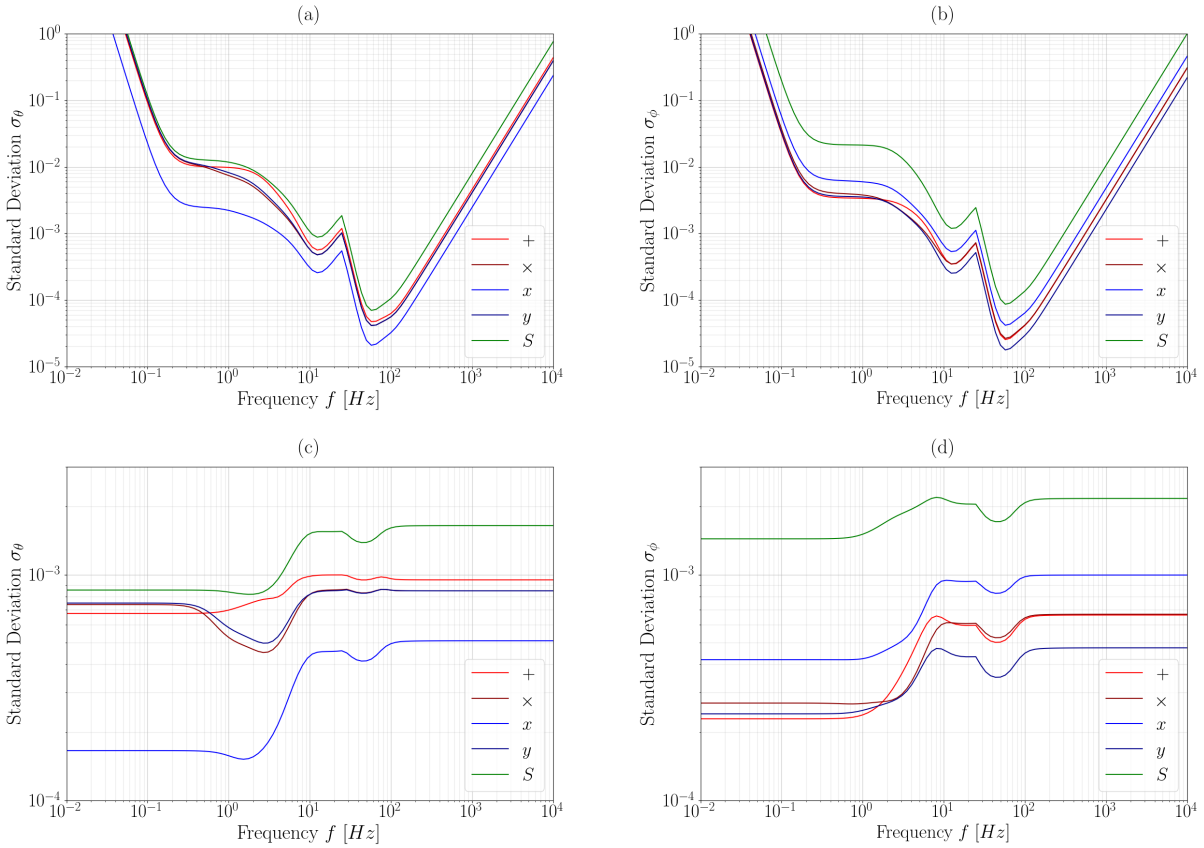

Figure 18: Frequency dependent standard deviation of θ and ϕ for a GW with amplitude $h = 10^{-25}$ in (a) and (b), and for twice the minimal amplituede of the scalar mode $h = 2|h_S|_{min}$, see Figure 17, in (c) and (d).

We plot the direction dependent sensitivities in Figure 19, using Eq. (91) along with the angular resolution for waves with these polarizations by taking the square root of Eq.(92) at a frequency of 100 Hz, where our set of detectors is most sensitive.

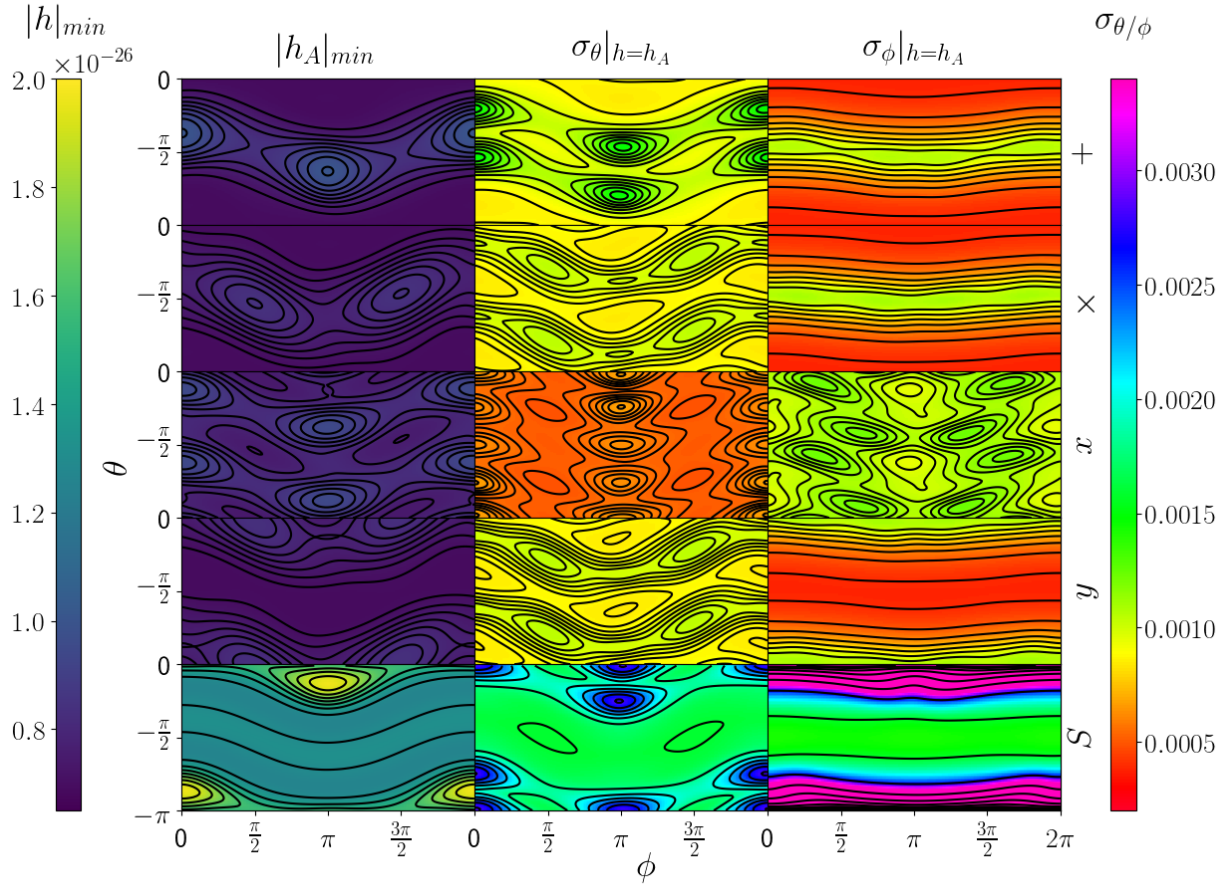

Figure 19: Sensitivity of ET, LIGO and DECIGO towards the polarizations $A \in \{+, \times, x, y, S\}$ in the left column. Standard deviation of the θ and ϕ angle for a GW with polarization A and amplitude of $h_A = 2 \cdot 10^{-26}$ in the middle and right column respectively.

In Figure 20 we plot the frequency dependent sensitivity of B-DECIGO together with ET and LIGO. The behaviour is very similar to the one with DECIGO, except that the plateau around 1 Hz is missing. Since B-DECIGO is not as sensitive as DECIGO it can only increase the sensitivity there a bit.

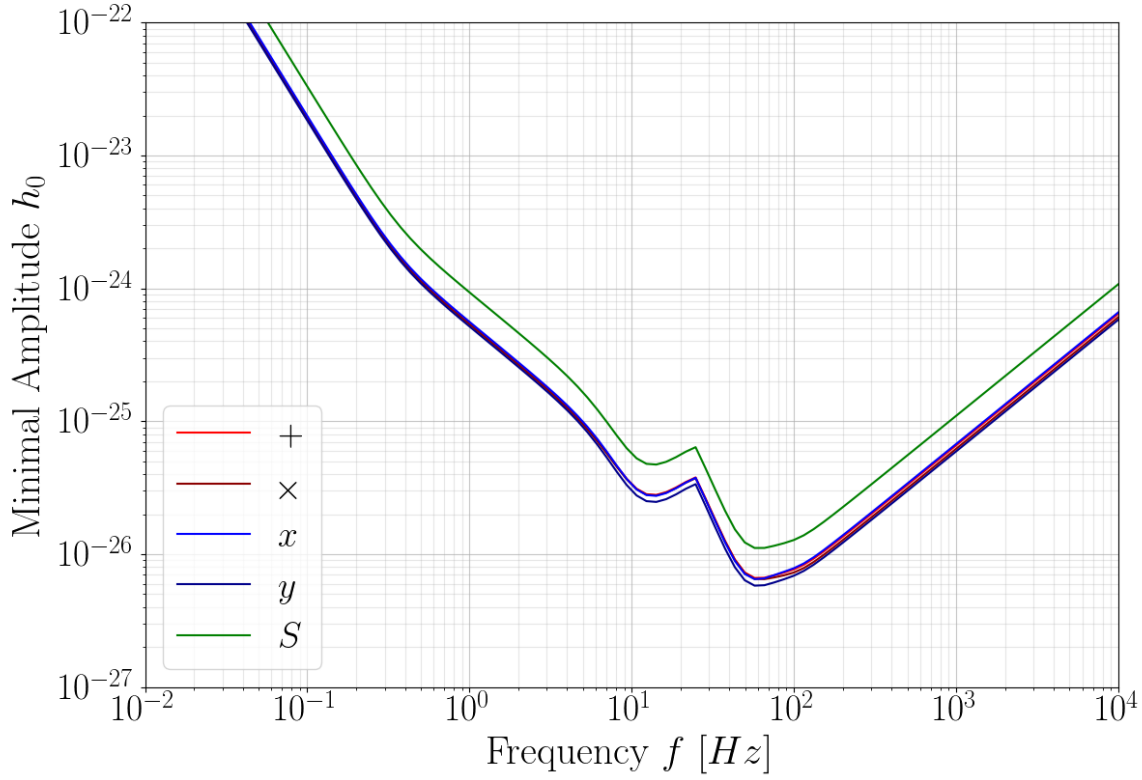

Figure 20: Frequency dependent sensitivity of ET, LIGO and B-DECIGO.

6 Conclusions

The Einstein Telescope is alone not sensitive to polarization modes, but one only needs one additional detector to change that. Small changes in ET geometry lead to no difference in the case of tilted planes and to a small sensitivity in case of a small change in the angles. So, it is questionable whether it is reasonable to do that.

By combining aLIGO, aVIRGO, KAGRA and ET one can detect a GWB with a strain amplitude below 10^{-27} and distinguish its polarization modes around a frequency of 100 Hz. One can enhance the sensitivity for lower frequencies by cross correlating with all DECIGO detectors of the C3 configuration. With this, one can measure strains of about 10^{-26} in a broad band from 0.1 Hz to 1000 Hz.

It is possible to use an alternative method to distinguish the modes by using the time dependence of the signals, with which one can clearly distinguish the scalar and vector modes by the blind spots, using the right detector pairs. This however does not work for B-DECIGO. Its time dependence is very chaotic since B-DECIGO angular frequency around Earth is an irrational fraction of Earth rotation and the distance to Earth detectors is varying relevantly. The sensitivities of the different modes are too close together, whenever the detectors are too close to Earth. This can be resolved however if one chooses an orbit on a higher altitude such that it circles the Earth once a day. In that case the method becomes more complicated than with the original DECIGO, but is still feasible.

With that we presented two methods with which we can use the already existing and planned detectors to test GR by measuring the polarizations of the GWB.

In a future project, one could investigate the possibilities of detecting inhomogeneities in the gravitational wave background analogue to the ones in the cosmic microwave background. Up to now we only calculated the minimal strain of a GW to be detected. But to find out how large the deviation from the mean would have to be to detect them, we would have to deal with the variance of the parameter estimation. It would be interesting to find out what angular resolution one could get with various detector combinations.
Gravitational waves should travel undisturbed since Planck time, which would make it possible to measure properties of the early quantum gravitational universe directly. This could give us valuable hints on the search of a unifying theory. This remarkable advantage of GW over the electromagnetic ones also has its disadvantages. Due to the enormous density of the early universe many emissions of GW would be expected from different epochs in the big bang. The difficulty would be to distinguish a signal of an earlier epoch from a later one. One of the most exciting things to do in the far future would be to create a complete gravitational map of the beginning of our universe.

A Delta distribution Approximation

In this Appendix we give a detailed derivation of the signal to noise ratio for a merger by focusing on the approximations of the Dirac delta distribution and the Fourier transforms. We first use a scalar signal, measured by two detectors, to simplify the calculation and then generalize to a wave with arbitrary polarizations measured by multiple detectors.
In future all GW detectors together could be sensitive enough to measure the in spiral of a binary Black Hole or neutron star merger, months before the merger event happens. In this case detectors with different distances from the source would have different observation times. This would help to measure the position of the source in the sky:

$$c\Delta T = \hat{\Omega} \cdot \Delta \vec{x}_{IJ}, \qquad \Delta T = T_I - T_J, \qquad \Delta \vec{x}_{IJ} = \vec{x}_I - \vec{x}_J, \tag{94}$$

where T_I and T_J are the observation times of the detectors I and J, $\vec{x}_I$ and $\vec{x}_J$ their position vectors and $\hat{\Omega}$ is the direction of travel of the GW.

We define the cross correlated and filtered strain amplitude of the detector pair (I, J) by:

$$Y \coloneqq \int_{-T_I/2}^{T_I/2} \int_{-T_J/2}^{T_J/2} s_I(t) s_J(t') Q(t - t') dt' dt, \tag{95}$$

where Q is the filter function and s_I, s_J are the strains measured by the detectors I,J, which are the sum of the signal h_I and the noise n_I in detector I:

$$s_I(t) = h_I(t) + n_I(t). \tag{96}$$

By taking the ensemble average we get rid of the noise terms:

$$\begin{aligned}
\mu &\coloneqq \mathbb{E}[Y] \\
&= \int_{-T_I/2}^{T_I/2} \int_{-T_J/2}^{T_J/2} \left\{ \mathbb{E}[h_I(t) h_J(t')] + \mathbb{E}[h_I(t) n_J(t')] + \mathbb{E}[n_I(t) h_J(t')] + \mathbb{E}[n_I(t) n_J(t')] \right\} Q(t - t') dt' dt \\
&= \int_{-T_I/2}^{T_I/2} \int_{-T_J/2}^{T_J/2} \int \tilde{h}_I^*(f) e^{2\pi i f \left(t - \frac{\hat{\Omega} \cdot \vec{x}_I}{c} \right)} df \int \tilde{h}_J(f') e^{-2\pi i f' \left(t' - \frac{\hat{\Omega} \cdot \vec{x}_J}{c} \right)} df' Q(t - t') dt' dt \\
&= \int \tilde{h}_I^*(f) \tilde{h}_J(f') e^{-\frac{2\pi i}{c} \hat{\Omega} \cdot (f \vec{x}_I - f' \vec{x}_J)} \int_{-T_I/2}^{T_I/2} \int_{-T_J/2}^{T_J/2} Q(t - t') e^{-2\pi i (f' t' - f t)} dt' dt df' df,
\end{aligned} \tag{97}$$

where we replaced the signal by its Fourier transform: $h_I(t) = \int \tilde{h}_I(f) e^{-2\pi i f \left(t - \frac{\hat{\Omega} \cdot \vec{x}_I}{c} \right)} df$.

We apply the following substitution to the integral over t': $\tau = t - t'$, $d\tau = dt$,

$$\mu = \int \tilde{h}_I^*(f) \tilde{h}_J(f') e^{-\frac{2\pi i}{c} \hat{\Omega} \cdot (f \vec{x}_I - f' \vec{x}_J)} \int_{-T_J/2}^{T_J/2} \int_{-T_I/2 - t'}^{T_I/2 - t'} Q(\tau) e^{2\pi i f \tau} d\tau e^{-2\pi i (f' - f) t'} dt' df' df. \tag{98}$$

Then we approximate the integral over τ with the Fourier transform of the filter function Q:

$$\int_{-T_I/2 - t'}^{T_I/2 - t'} Q(\tau) e^{2\pi i f \tau} d\tau \approx \tilde{Q}(f). \tag{99}$$

If we shift a wave packed in time, it is still composed of the same frequencies. Therefore, we can ignore the time shift in the integration volume by $-t$.

We pull this out of the t integral and get:

$$\int_{-T_J/2}^{T_J/2} e^{-2\pi i(f'-f)t'}dt' = -\frac{1}{\pi\Delta f}\frac{1}{2i}\left(e^{-\pi i\Delta f T_J} - e^{\pi i\Delta f T_J}\right) = \frac{\sin(\pi\Delta f T_J)}{\pi\Delta f} =: \delta_{T_J}(f'-f). \quad (100)$$

If $\Delta f = f' - f$ approaches zero, we get: $\lim_{\Delta f\to 0}\delta_{T_J}(\Delta f) = \lim_{\Delta f\to 0}\frac{1}{\pi\Delta f}(0 + \pi T_J\Delta f + \mathcal{O}(\Delta f^2)) = T_J$ and for big Δf, δ_{T_J} gets small:

$$\left|\frac{\sin(\pi\Delta f T_J)}{\pi\Delta f}\right| \leqslant \frac{1}{\pi\Delta f} \overset{\Delta f\to\infty}{\longrightarrow} 0. \quad (101)$$

By approximating $\delta_{T_J}(f'-f) \approx \delta(f'-f)$ with the Dirac delta distribution we can evaluate the integral over f'.

$$\mu \approx \int \tilde{h}_I^*(f)\tilde{h}_J(f')e^{-\frac{2\pi i}{c}\hat{\Omega}\cdot(f\vec{x}_I - f'\vec{x}_J)}\tilde{Q}(f')\delta(f'-f)df'df = \int \tilde{h}_I^*(f)\tilde{h}_J(f)\tilde{Q}(f)e^{-2\pi i f\frac{\hat{\Omega}\cdot\Delta\vec{x}_{IJ}}{c}}df. \quad (102)$$

We now have an expression for the signal. To calculate the signal to noise ratio we need to deal with noise which is the square root of the variance in absence of a signal:

$$\begin{aligned}\sigma^2 &\coloneqq \mathbb{V}[Y]|_{h=0} = \mathbb{E}[Y^2] - \mathbb{E}[Y]^2|_{h=0} = \mathbb{E}[Y^2]|_{h=0} \\ &= \int_{-T_I/2}^{T_I/2}\int_{-T_I/2}^{T_I/2}\int_{-T_J/2}^{T_J/2}\int_{-T_J/2}^{T_J/2}\mathbb{E}[s_I(t)s_I(t')s_J(\tau)s_J(\tau')]Q(t-\tau)Q(t'-\tau')d\tau' d\tau dt' dt|_{h=0} \\ &= \int_{-T_I/2}^{T_I/2}\int_{-T_I/2}^{T_I/2}\int_{-T_J/2}^{T_J/2}\int_{-T_J/2}^{T_J/2}\mathbb{E}[n_I(t)n_I(t')]\mathbb{E}[n_J(\tau)n_J(\tau')]Q(t-\tau)Q(t'-\tau')d\tau' d\tau dt' dt. \quad (103)\end{aligned}$$

Since the noises of the two detectors are independent of each other, we can take their expectation separately. We then insert the Fourier transformation (FT) of the noise, in the time interval in which the measurement is taken:

$$n_I(t) = \int \tilde{n}_I(f)e^{-2\pi i f t}df, \quad (104)$$

And then swap the time and frequency integrals and approximate the FT of the filter function and the delta distribution as before:

$$\begin{aligned}\sigma^2 &= \int \mathbb{E}[\tilde{n}_I^*(f)\tilde{n}_I(f')]\mathbb{E}[\tilde{n}_J(\nu)\tilde{n}_J^*(\nu')]\tilde{Q}(\nu)\delta(\nu-f)\tilde{Q}^*(\nu')\delta(\nu'-f')d\nu' d\nu df' df \\ &= \int \mathbb{E}[\tilde{n}_I^*(f)\tilde{n}_I(f')]\mathbb{E}[\tilde{n}_J(f)\tilde{n}_J^*(f')]\tilde{Q}(f)\tilde{Q}^*(f')df' df. \quad (105)\end{aligned}$$

Now we use that different frequencies in the noise are not correlated to each other and the definition of the two sided noise power spectral density:

$$\mathbb{E}[\tilde{n}_I^*(f)\tilde{n}_I(f')] =: \frac{1}{2}P_I(|f'|)\delta(f'-f). \quad (106)$$

If we would carelessly plug in this identity, we would get a multiplication of two delta distributions, which is not definable. But we cannot take the expectation of the noise squared over an infinite

time integral anyway. So, the delta distribution is actually a δ_{T_I}. This is a smooth function and not a distribution and can therefore be multiplied with another δ_{T_J}.

$$\begin{aligned}\sigma^2 &= \frac{1}{4}\int P_I(|f'|)P_J(|f'|)\tilde{Q}(f)\tilde{Q}^*(f')\int_{-T_I/2}^{T_I/2} e^{-2\pi i(f'-f)t}dt\int_{-T_J/2}^{T_J/2} e^{2\pi i(f'-f)t'}dt'df'df \\ &= \frac{1}{4}\int P_I(|f'|)P_J(|f'|)\tilde{Q}(f)\tilde{Q}^*(f')\int_{-T_I/2}^{T_I/2}\int_{-T_J/2}^{T_J/2} e^{2\pi i(f'-f)(t'-t)}dt'dtdf'df. \end{aligned} \tag{107}$$

To evaluate the time integrals we have to split the integration domain into three regions as depicted in Figure 21, since we need an integration region which is symmetric around $t'-t=0$, where we can use Eq. (100). The rest can be evaluated separately.

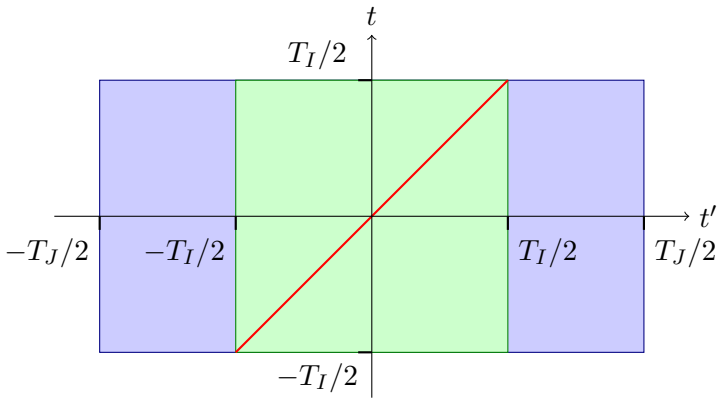

Figure 21: The green region is symmetric around $t'-t=0$ (red line). The blue rectangle marks the entire integration region.

Let $T_I < T_J$, $\Delta T = T_J - T_I$ and $\Delta f = f' - f$, then the time integrals read:

$$\delta_{T_I}\delta_{T_J} = \int_{-T_I/2}^{T_I/2}\int_{-T_J/2}^{-T_I/2} e^{-2\pi i\Delta f(t'-t)}dt' + \int_{-T_I/2}^{T_I/2} e^{-2\pi i\Delta f(t'-t)}dt' + \int_{T_I/2}^{T_J/2} e^{-2\pi i\Delta f(t'-t)}dt'dt. \tag{108}$$

We substitute $\eta = -t'$ in the first inegral over t', to bring it into the same form as the third one.

$$\begin{aligned}\delta_{T_I}\delta_{T_J} &= \int_{-T_I/2}^{T_I/2} - \int_{T_J/2}^{T_I/2} e^{2\pi i\Delta f(\eta+t)}d\eta + \int_{T_I/2}^{T_J/2} e^{-2\pi i\Delta f(t'-t)}dt'dt + \int_{-T_I/2}^{T_I/2}\int_{-T_I/2}^{T_I/2} e^{-2\pi i\Delta f(t'-t)}dt'dt \\ &= \int_{-T_I/2}^{T_I/2} e^{2\pi i\Delta ft}\int_{T_I/2}^{T_J/2} e^{2\pi i\Delta ft'} + e^{-2\pi i\Delta ft'}dt'dt + \delta_{T_I}^2(\Delta f) \\ &= \int_{-T_I/2}^{T_I/2} e^{2\pi i\Delta ft}dt\int_{T_I/2}^{T_J/2} 2\cos(2\pi\Delta ft')dt' + \delta_{T_I}^2(\Delta f) \\ &= \delta_{T_I}(\Delta f)\left(\frac{\sin(\pi\Delta fT_J) - \sin(\pi\Delta fT_I)}{\pi\Delta f} + \delta_{T_I}(\Delta f)\right) \\ &\approx \delta(f'-f)\left(\frac{\sin(\pi\Delta fT_I) + \pi\Delta f\Delta T + \mathcal{O}((\pi\Delta f\Delta T)^2) - \sin(\pi\Delta fT_I)}{\pi\Delta f} + \delta_{T_I}(\Delta f)\right), \end{aligned} \tag{109}$$

where we assumed, that $\Delta T \ll T_I$.

This approximated distribution acts on functions as follows:

$$\int g(f')\delta_{T_I}\delta_{T_J}(\Delta f)df' \approx \int g(f')\left(\Delta T + \mathcal{O}(f'-f) + \delta_{T_I}(f'-f)\right)\delta(f'-f)df = g(f)(T_I+\Delta T), \tag{110}$$

$\forall g \in C^\infty(\mathbb{C})$.

Inserting this into the variance and integrating over f' we get:

$$\begin{aligned}\sigma^2 &= \frac{1}{4}\int P_I(|f'|)P_J(|f'|)\tilde{Q}(f)\tilde{Q}^*(f')\delta_{T_I}\delta_{T_J}(f'-f)df'df \\ &= \frac{T_I+\Delta T}{4}\int P_I(|f|)P_J(|f|)|\tilde{Q}(f)|^2 df.\end{aligned} \tag{111}$$

Using matched filtering with the scalar product: $(\tilde{A},\tilde{B}) \coloneqq \int \tilde{A}^*(f)\tilde{B}(f)P_I(|f|)P_J(|f|)df$,
leads us to a filter function:

$$\tilde{Q}(f) = \frac{\tilde{h}_I^*(f)\tilde{h}_J(f)e^{2\pi i f\frac{\hat{\Omega}\cdot\Delta\vec{x}_{IJ}}{c}}}{P_I(|f|)P_J(|f|)}. \tag{112}$$

We can write the signal and noise in terms of the filter function and arrive at the signal to noise ratio:

$$SNR = \frac{\mu}{\sigma} = \frac{(\tilde{Q},\tilde{Q})}{\sqrt{\frac{T_I+\Delta T}{4}(\tilde{Q},\tilde{Q})}} = 2\sqrt{\frac{1}{T_I+\Delta T}\int \frac{|\tilde{h}_I(f)\tilde{h}_J(f)|^2}{P_I(|f|)P_J(|f|)}df}. \tag{113}$$

We now model the merger as a periodic source, which stops radiating at the end of the merging event at its time coordinate t_0. Under the assumption that the detectors are far away from the source, we can model the incoming wave as a plane wave with amplitude h_0 and frequency f_0, traveling in direction $\hat{\Omega}$:

$$h(t) = h_0 e^{2\pi i f_0(t-\frac{\hat{\Omega}\cdot\vec{x}}{c})}\theta\left(t_0 - \frac{\hat{\Omega}\cdot\vec{x}}{c} - t\right). \tag{114}$$

The detector I will measure the signal over a time period T_I and the Fourier transform of the measured signal is therefore:

$$\tilde{h}_I(f) = \int_{-T_I/2}^{T_I/2} h_0 e^{2\pi i f_0(t-\frac{\hat{\Omega}\cdot\vec{x}}{c})}e^{-2\pi i f t}dt = h_0 e^{-2\pi i f_0\frac{\hat{\Omega}\cdot\vec{x}}{c}}\int_{-T_I/2}^{T_I/2} e^{-2\pi i(f-f_0)t}dt \tag{115}$$

Again, we cannot approximate this with a delta distribution, otherwise we would get a δ^4 for the $|\tilde{h}_I\tilde{h}_J|^2$ term.

$$|\tilde{h}_I(f)\tilde{h}_J(f)|^2 = h_0^4\int_{-T_I/2}^{T_I/2}\int_{-T_I/2}^{T_I/2}\int_{-T_J/2}^{T_J/2}\int_{-T_J/2}^{T_J/2} e^{-2\pi i(f-f_0)(t'-t+\tau'-\tau)}d\tau' d\tau dt' dt. \tag{116}$$

We do the same splitting of the T_J interval as above, under the assumption $T_I < T_J$ and using the

short hand $\rho = t' - t + \tau' - \tau$:

$$
\begin{aligned}
|\tilde{h}_I \tilde{h}_J|^2 \propto \delta^2_{T_I}\delta^2_{T_J} &= \int_{-T_I/2}^{T_I/2}\int_{-T_J/2}^{T_J/2} e^{-2\pi i(f'-f)(t'-t+\tau'-\tau)} d\tau' d\tau dt' dt \\
&= \int_{-T_I/2}^{T_I/2}\int_{-T_J/2}^{-T_I/2} e^{-2\pi i\Delta f\rho} d\tau' d\tau + \int_{-T_I/2}^{T_I/2} e^{-2\pi i\Delta f\rho} d\tau' d\tau + \int_{T_I/2}^{T_J/2} e^{-2\pi i\Delta f\rho} d\tau' d\tau dt' dt \\
&= \int_{-T_I/2}^{T_I/2} e^{-2\pi i\Delta f(t'-t)} dt' dt \int_{T_I/2}^{T_J/2} e^{2\pi i\Delta f(\tau'-\tau)} + e^{-2\pi i\Delta f(\tau'-\tau)} d\tau' d\tau + \int_{-T_I/2}^{T_I/2} e^{-2\pi i\Delta f\rho} d\tau' d\tau dt' dt \\
&= \delta^2_{T_I}(\Delta f) \int_{T_I/2}^{T_J/2} 2\cos(2\pi\Delta f(\tau'-\tau)) d\tau' d\tau + \delta^4_{T_I}(\Delta f) \\
&= \delta^2_{T_I}(\Delta f) \left(\frac{1}{\pi\Delta f} \int_{T_I/2}^{T_J/2} \sin(\pi\Delta f(T_J - 2\tau)) - \sin(\pi\Delta f(T_I - 2\tau)) d\tau + \delta^2_{T_I}(\Delta f) \right) \\
&= \delta^2_{T_I}(\Delta f) \left(-\frac{1}{2(\pi\Delta f)^2} \{\cos(\pi\Delta f(T_J - T_J)) - \cos(\pi\Delta f(T_J - T_I)) \right. \\
&\qquad \left. - \cos(\pi\Delta f(T_I - T_J)) + \cos(\pi\Delta f(T_I - T_I))\} + \delta^2_{T_I}(\Delta f) \right) \\
&= \delta^2_{T_I}(\Delta f) \left(\frac{1}{(\pi\Delta f)^2} \{\cos(\pi\Delta f\Delta T) - 1\} + \delta^2_{T_I}(\Delta f) \right) \\
&= \delta(f'-f)\delta_{T_I}(\Delta f) \left(\frac{1}{(\pi\Delta f)^2} \left\{ 1 - \frac{1}{2}(\pi\Delta f\Delta T)^2 + \mathcal{O}(\Delta f^4) - 1 \right\} + \delta^2_{T_I}(\Delta f) \right). \qquad (117)
\end{aligned}
$$

The action on a function $g \in C^\infty(\mathbb{C})$ is:

$$
\begin{aligned}
\int g(f')\delta^2_{T_I}\delta^2_{T_J}(f'-f)df' &= \int g(f')\delta_{T_I}(\Delta f) \left(\frac{\Delta T^2}{2} + \mathcal{O}(\Delta f^2) + \delta_{T_I}(\Delta f)^2 \right) \delta(f'-f) df' \\
&= g(f)\delta_{T_I}(0) \left(\frac{\Delta T^2}{2} + \delta_{T_I}(0)^2 \right) = g(f) T_I \left(\frac{\Delta T^2}{2} + T_I^2 \right). \qquad (118)
\end{aligned}
$$

When we plug this into the SNR we get:

$$
SNR = 2\sqrt{\frac{T_I}{T_I + \Delta T} \left(\frac{\Delta T^2}{2} + T_I^2 \right) \frac{h_0^4}{P_I(|f_0|)P_J(|f_0|)}} \approx 2 \left(T_I + \frac{\hat{\Omega} \cdot \Delta\vec{x}_{IJ}}{2c} \right) \frac{h_0^2}{\sqrt{P_I(f_0)P_J(f_0)}}, \quad (119)
$$

where we used the identification of the integration time with the direction of the source in Eq. (94).

The minimal amplitude is then given by:

$$
h_{min} = \sqrt{32} \left(\frac{(T_I + \Delta T)P_I(f)P_J(f)}{T_I \left(\frac{\Delta T^2}{2} + T_I^2 \right)} \right)^{\frac{1}{4}} \approx \sqrt{32} \left(\frac{1}{\sqrt{T_I}} + \frac{\hat{\Omega} \cdot \Delta\vec{x}_{IJ}}{4c\sqrt{T_I}^3} \right) \sqrt[4]{P_I(f)P_J(f)}. \qquad (120)
$$

Including polarizations, we have a gravitational wave $h_{ij}(t)$, which induces the signal $h_I(t)$ in

detector I:

$$h_{ij}(t) = \sum_A h_A e^{2\pi i f_0(t-\frac{\hat{\Omega}\cdot\vec{x}}{c})+\varphi_A}\theta\left(t_0 - \frac{\hat{\Omega}\cdot\vec{x}}{c} - t\right)e^A_{ij} \tag{121}$$

$$h_I(t) = \sum_A h_A F^A_I(\hat{\Omega}) e^{2\pi i f_0(t-\frac{\hat{\Omega}\cdot\vec{x}_I}{c})+\varphi_A}\theta\left(t_0 - \frac{\hat{\Omega}\cdot\vec{x}_I}{c} - t\right), \tag{122}$$

where h_A is the amplitude of the wave in polarization A and φ_A accounts for the fact that the polarizations could be phase shifted.
For the absolute value squared of the cross correlated signals of two detectors we get:

$$\begin{aligned}
&|\tilde{h}_I(f)\tilde{h}_J(f)|^2 = |\tilde{h}_I(f)|^2|\tilde{h}_J(f)|^2 \\
&= \left|\sum_A h_A F^A_I(\hat{\Omega}) e^{-\frac{2\pi i f_0}{c}\hat{\Omega}\cdot\vec{x}_I+i\varphi_A}\right|^2 \left|\sum_A h_A F^A_J(\hat{\Omega}) e^{-\frac{2\pi i f_0}{c}\hat{\Omega}\cdot\vec{x}_J+i\varphi_A}\right|^2 \int_{-T_I/2}^{T_I/2}\int_{-T_J/2}^{T_J/2} e^{-2\pi i(f-f_0)\rho} d^4\rho \\
&= \left|\sum_A h_A F^A_I(\hat{\Omega}) e^{i\varphi_A}\right|^2 \left|\sum_A h_A F^A_J(\hat{\Omega}) e^{i\varphi_A}\right|^2 \delta_{T_I}(f-f_0)\left(\frac{\Delta T^2}{2} + \delta_{T_I}(f-f_0)^2\right).
\end{aligned} \tag{123}$$

We make the assumption, that the gravitational wave has only one of the polarizations $h = \sum_{A'} h_{A'}\delta_{A'A}$, to get the signal to noise ratio for that polarization.

$$\begin{aligned}
SNR_A &\coloneqq \frac{\mu}{\sigma}\Big|_{h=h_A} = 2\sqrt{\frac{T_I}{T_I+\Delta T}\left(\frac{\Delta T^2}{2}+T_I^2\right)\frac{(|h_A|^2 F^A_I(\hat{\Omega})F^A_J(\hat{\Omega}))^2}{P_I(|f_0|)P_J(|f_0|)}} \\
&\approx 2\left(T_I + \frac{\hat{\Omega}\cdot\Delta\vec{x}_{IJ}}{2c}\right)\frac{|h_A|^2 F^A_I(\hat{\Omega})F^A_J(\hat{\Omega})}{\sqrt{P_I(f_0)P_J(f_0)}},
\end{aligned} \tag{124}$$

which we get by replacing $h_0^4 \mapsto (|h_A|^2 F^A_I(\hat{\Omega})F^A_J(\hat{\Omega}))^2$ in Eq. (119).

For multiple detectors we use the maximum likelihood method and calculate the Fisher matrix. The likelihood function is given by:

$$L(\mu_{IJ},\vec{\theta}) = e^{-\sum_{(I,J)}\frac{(Y_{IJ}-\mu_{IJ})^2}{2\sigma^2_{IJ}}}, \tag{125}$$

where $\mu_{IJ} = \mathbb{E}[Y_{IJ}]$ is the ensemble average of the correlated signals of the detectors I and J. Its variance $\sigma^2_{IJ} = \mathbb{V}[Y_{IJ}]$ is given by Eq. (111) without the filtering. Multiplying the SNR Eq. (119) with the noise we get:

$$\mu_{IJ} = \sqrt{T_I\left(\frac{\Delta T^2}{2}+T_I^2\right)}|\tilde{h}_I\tilde{h}_J|. \tag{126}$$

The matrix element $F_{AA'}$ of the Fisher matrix is then given by:

$$\begin{aligned}
F_{AA'} &= \mathbb{E}\left[\left(\partial_{|h_A|^2} \ln L\right)\left(\partial_{|h_{A'}|^2} \ln L\right)\right] \\
&= \mathbb{E}\left[\left(\sum_{(I,J)} \frac{1}{\sigma_{IJ}^2}(Y_{IJ}-\mu_{IJ})\sqrt{T_I\left(\frac{\Delta T^2}{2}+T_I^2\right)}\right)^2 \left(\partial_{|h_A|^2}|\tilde{h}_I\tilde{h}_J|\right)\left(\partial_{|h_{A'}|^2}|\tilde{h}_I\tilde{h}_J|\right)\right] \\
&= \sum_{(I,J)} \frac{1}{\sigma_{IJ}^4}\underbrace{\mathbb{E}[(Y_{IJ}-\mu_{IJ})^2]}_{\mathbb{V}[Y_{IJ}]=\sigma_{IJ}^2} T_I\left(\frac{\Delta T^2}{2}+T_I^2\right)\left(\partial_{|h_A|^2}|\tilde{h}_I\tilde{h}_J|\right)\left(\partial_{|h_{A'}|^2}|\tilde{h}_I\tilde{h}_J|\right) \\
&\quad + \sum_{(I,J)\neq(I',J')} \frac{1}{\sigma_{IJ}^2\sigma_{I'J'}^2}\underbrace{\mathbb{E}[(Y_{IJ}-\mu_{IJ})(Y_{I'J'}-\mu_{I'J'})]}_{Cov(Y_{IJ},Y_{I'J'})=0} T_I\left(\frac{\Delta T^2}{2}+T_I^2\right)\left(\partial_{|h_A|^2}|\tilde{h}_I\tilde{h}_J|\right)\left(\partial_{|h_{A'}|^2}|\tilde{h}_{I'}\tilde{h}_{J'}|\right) \\
&= \sum_{(I,J)} \frac{4T_I}{(T_I+\Delta T)P_IP_J}\left(\frac{\Delta T^2}{2}+T_I^2\right)\left(\partial_{|h_A|^2}|\tilde{h}_I\tilde{h}_J|\right)\left(\partial_{|h_{A'}|^2}|\tilde{h}_I\tilde{h}_J|\right) \qquad (127)
\end{aligned}$$

The SNR squared of a specific polarization A is defined by dividing the square of the quantity we are looking for $|h_A|^2$ by its variance σ_A, under the condition that the incoming wave has only that polarization.

$$SNR_A^2 \coloneqq \left.\frac{(|h_A|^2)^2}{\sigma_A^2}\right|_{h=h_A} = \left.\frac{(|h_A|^2)^2}{(F^{-1})_{AA}}\right|_{h=h_A} = \left.\frac{(|h_A|^2)^2\det\mathbf{F}}{\mathcal{F}_A}\right|_{h=h_A} \qquad (128)$$

B Fisher matrix entries

As can be seen in Appendix A, the Fisher matrix can be written as a sum of Fisher matrices of single detector pairs, which consist of a pre-factor and two derivative terms for row and column of the entry. If $\theta_{i,j}$ are polarizations we have:

$$F_{ij} \propto \left(\partial_{\theta_i}|\tilde{h}_I\tilde{h}_J|\right)\left(\partial_{\theta_j}|\tilde{h}_I\tilde{h}_J|\right), \qquad (129)$$

where $\vec{\theta} = (\theta, \phi, +, \times, x, y, b, l)$ are the parameters we are looking for.

Here we calculate those derivative terms.
We start by writing out the absolute value squared of the correlation signal.

$$|\tilde{h}_I\tilde{h}_J|^2 = \left|\sum_A h_A F_I^A \sum_{A'} h_{A'} F_J^{A'}\right|^2, \qquad (130)$$

where the phase φ_A of the polarization A is integrated in the complex valued amplitude $h_A \in \mathbb{C}$.
We split the multiplied signals up into sums over terms where the polarizations coincide and where

they are different:

$$
\begin{aligned}
|\tilde{h}_I\tilde{h}_J|^2 &= \left|\sum_A h_A^2 F_I^A F_J^A + \sum_{A\neq A'} h_A h_{A'} F_I^A F_J^{A'}\right|^2 \\
&= \left(\sum_A h_A^2 F_I^A F_J^A\right)\left(\sum_B h_B^2 F_I^B F_J^B\right)^* + \left(\sum_A h_A^2 F_I^A F_J^A\right)\left(\sum_{B\neq B'} h_B h_{B'} F_I^B F_J^{B'}\right)^* \\
&\quad + \left(\sum_{A\neq A'} h_A h_{A'} F_I^A F_J^{A'}\right)\left(\sum_B h_B^2 F_I^B F_J^B\right)^* + \left(\sum_{A\neq A'} h_A h_{A'} F_I^A F_J^{A'}\right)\left(\sum_{B\neq B'} h_B h_{B'} F_I^B F_J^{B'}\right)^* \\
&= \sum_A \left(|h_A|^2 F_I^A F_J^A\right)^2 + \sum_{A\neq B}(h_A h_B^*)^2 F_I^A F_J^A F_I^B F_J^B \\
&\quad + \sum_A h_A |h_A|^2 F_I^A F_J^A \sum_{B\neq A} h_B^*(F_I^A F_J^B + F_I^B F_J^A) + \sum_{A\neq B\neq B'} h_A^2 F_I^A F_J^A h_B^* h_{B'}^* F_I^B F_J^{B'} \\
&\quad + \sum_B h_B^* |h_B|^2 F_I^B F_J^B \sum_{A\neq B} h_A(F_I^B F_J^A + F_I^A F_J^B) + \sum_{A\neq A'\neq B} h_A h_{A'} F_I^A F_J^{A'} (h_B^*)^2 F_I^B F_J^B \\
&\quad + \sum_{A\neq A'} |h_A|^2 |h_{A'}|^2 \left[(F_I^A F_J^{A'})^2 + F_I^A F_J^{A'} F_I^{A'} F_J^A\right] \\
&\quad + \sum_A |h_A|^2 \sum_{\substack{B\neq B' \\ B,B'\neq A}} h_B h_{B'}^* \left[(F_I^A)^2 F_J^B F_J^{B'} + F_I^A F_J^A (F_I^B F_J^{B'} + F_I^{B'} F_J^B) + (F_J^A)^2 F_I^B F_I^{B'}\right] \\
&\quad + \sum_{A\neq A'\neq B\neq B'} h_A h_{A'} h_B^* h_{B'}^* F_I^A F_J^{A'} F_I^B F_J^{B'}. \qquad (131)
\end{aligned}
$$

When we take the derivative after $|h_A|^2$ all sums which do not contain such a term vanish.

$$
\begin{aligned}
\partial_{|h_A|^2}|\tilde{h}_I\tilde{h}_J| &= \frac{1}{2\sqrt{|\tilde{h}_I\tilde{h}_J|}}\Bigg\{ 2|h_A|^2(F_I^A F_J^A)^2 + h_A F_I^A F_J^A \sum_{B\neq A} h_B^*(F_I^A F_J^B + F_I^B F_J^A) \\
&\quad + h_A^* F_I^A F_J^A \sum_{B\neq A} h_B(F_I^A F_J^B + F_I^B F_J^A) + \sum_{A'\neq A} |h_{A'}|^2 \left[(F_I^A F_J^{A'})^2 + 2F_I^A F_J^{A'} F_I^{A'} F_J^A + (F_I^{A'} F_J^A)^2\right] \\
&\quad + \sum_{\substack{B\neq B' \\ B,B'\neq A}} h_B h_{B'}^* \left[(F_I^A)^2 F_J^B F_J^{B'} + F_I^A F_J^A (F_I^B F_J^{B'} + F_I^{B'} F_J^B) + (F_J^A)^2 F_I^B F_I^{B'}\right]\Bigg\}. \qquad (132)
\end{aligned}
$$

We add the condition, that we have an incoming wave with polarization A_0 and therefore all terms proportional to two different polarizations are zero.

$$
\begin{aligned}
\partial_{|h_A|^2}|\tilde{h}_I\tilde{h}_J|\Big|_{h=h_{A_0}} &= \frac{1}{2\sqrt{\left(|h_{A_0}|^2 F_I^{A_0} F_J^{A_0}\right)^2 + 0}}\Big\{2\delta_{AA_0}|h_A|^2(F_I^A F_J^A)^2 \\
&\quad + (1-\delta_{AA_0})|h_{A_0}|^2\left[(F_I^A F_J^{A_0})^2 + 2F_I^A F_J^{A_0} F_I^{A_0} F_J^A + (F_I^{A_0} F_J^A)^2\right]\Big\} \\
&= F_I^A F_J^A + (1-\delta_{AA_0})\frac{1}{2}\left[\frac{(F_I^A)^2 F_J^{A_0}}{F_I^{A_0}} + \frac{(F_J^A)^2 F_I^{A_0}}{F_J^{A_0}}\right] \qquad (133)
\end{aligned}
$$

If we calculate a matrix element in the θ or ϕ row or column, we cannot pull the term $\sqrt{T_I\left(\frac{\Delta T^2}{2}+T_I^2\right)}$ out in front, so the general Fisher matrix element looks like:

$$\begin{aligned} F_{ij} &= \mathbb{E}\left[(\partial_{\theta_i}\ln L)(\partial_{\theta_j}\ln L)\right] \\ &= \sum_{(I,J)}\frac{1}{\sigma_{IJ}^2}\left(\partial_{\theta_i}\sqrt{T_I\left(\frac{\Delta T^2}{2}+T_I^2\right)}|\tilde{h}_I\tilde{h}_J|\right)\left(\partial_{\theta_j}\sqrt{T_I\left(\frac{\Delta T^2}{2}+T_I^2\right)}|\tilde{h}_I\tilde{h}_J|\right) \end{aligned} \tag{134}$$

The variance of the true signal Y_{IJ} is dependent on the true time difference and we can treat it as a parameter when we take the derivative after the estimated θ-value.

$$\mathbb{V}[Y_{IJ}] = \sigma_{IJ}^2 = \frac{T_I+\Delta T}{4}P_IP_J, \qquad \Delta T = \frac{\hat{\omega}\cdot\Delta\vec{x}_{IJ}}{c}, \tag{135}$$

where $\hat{\omega}$ is the true direction of the source.

The derivative term for the angle θ for a wave with polarization A_0 is given by:

$$\begin{aligned} \partial_\theta\sqrt{T_I\left(\frac{\Delta T^2}{2}+T_I^2\right)}|\tilde{h}_I\tilde{h}_J|\Big|_{h=h_{A_0}} =& \frac{T_I\Delta T}{2\sqrt{T_I\left(\frac{\Delta T^2}{2}+T_I^2\right)}}\frac{\hat{\Omega}_{,\theta}\cdot\Delta\vec{x}_{IJ}}{c}|h_{A_0}|^2F_I^{A_0}F_J^{A_0} \\ &+\sqrt{T_I\left(\frac{\Delta T^2}{2}+T_I^2\right)}|h_{A_0}|^2\left(F_{I,\theta}^{A_0}F_J^{A_0}+F_I^{A_0}F_{J,\theta}^{A_0}\right) \end{aligned} \tag{136}$$

C Provisory Pictures

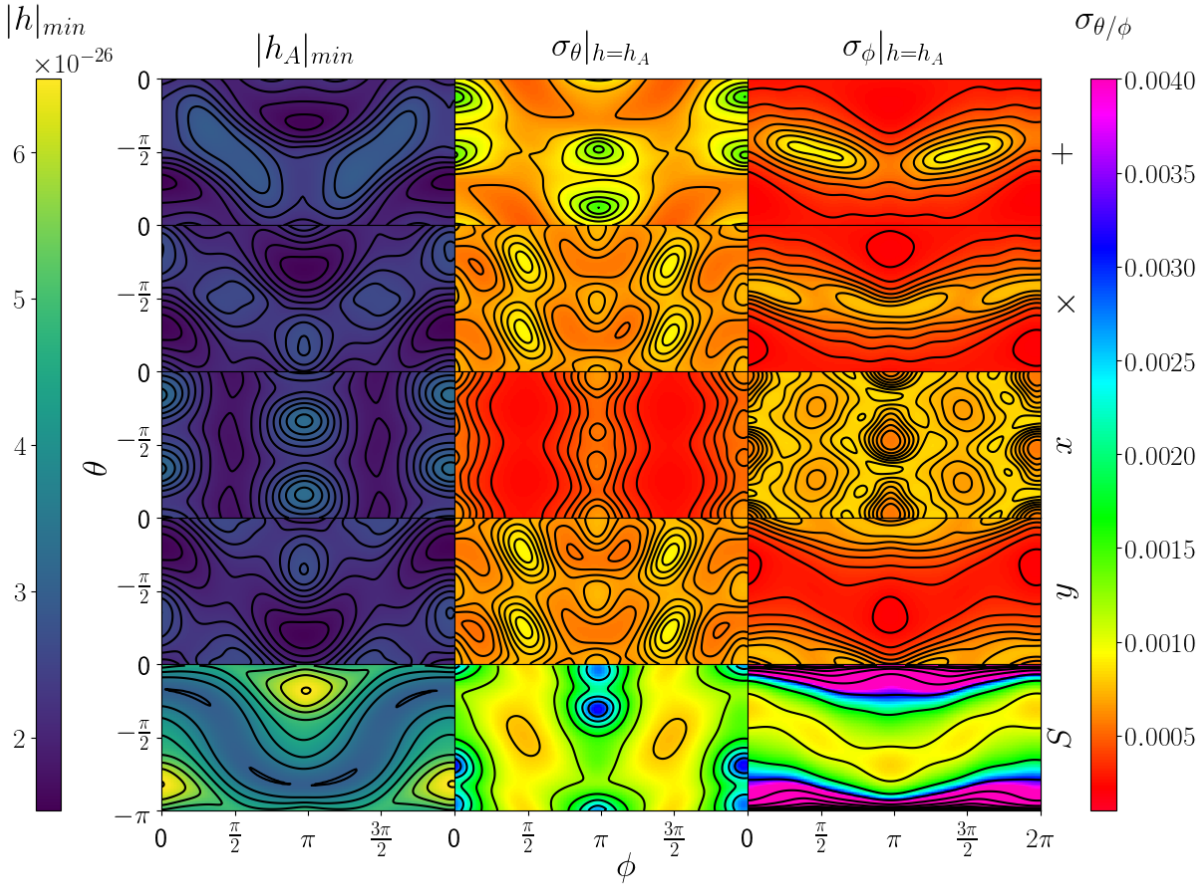

Figure 22: Angular dependence of the sensitivity to polarizations and standard deviation of θ and ϕ at 10 Hz.

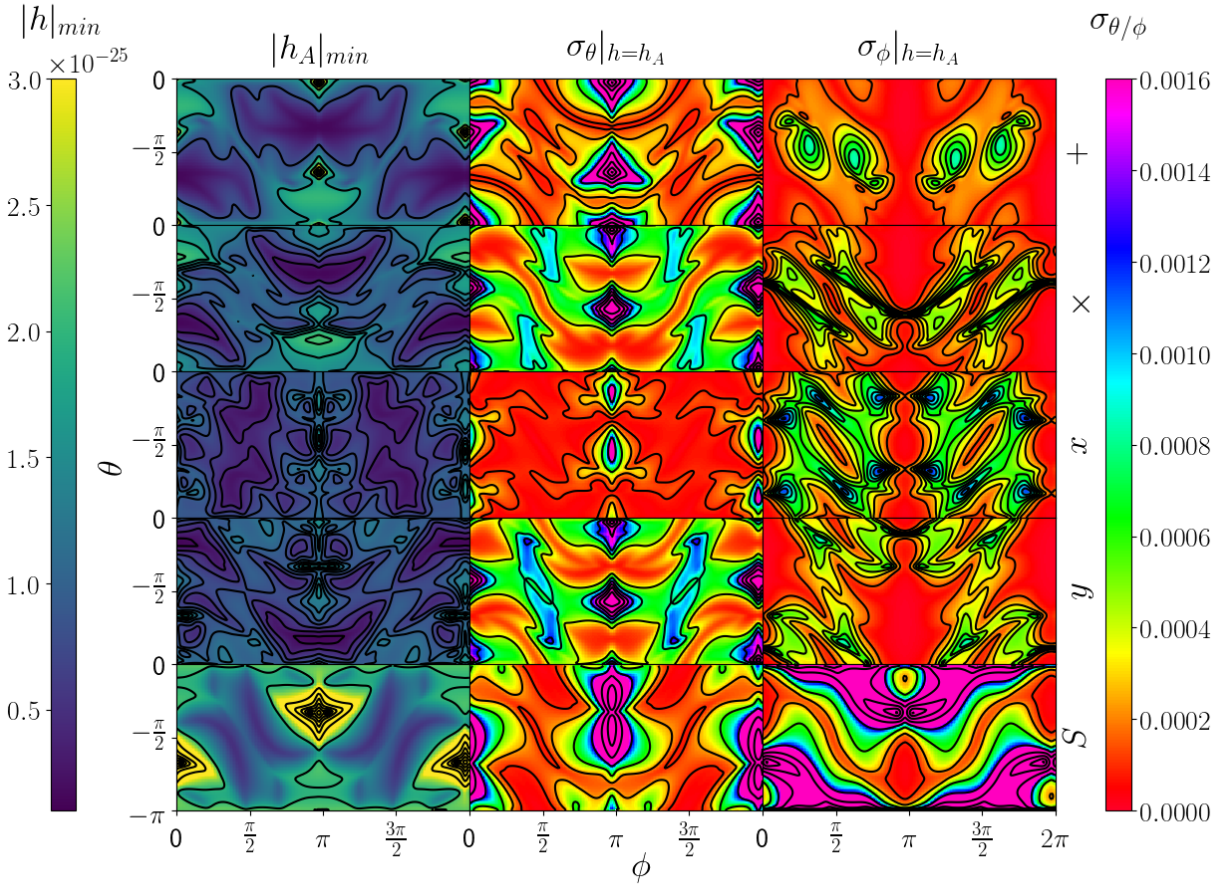

Figure 23: Angular dependence of the sensitivity to polarizations and standard deviation of θ and ϕ at 1 Hz.

References

[1] LIGO Scientific Collaboration and Virgo Collaboration, Phys. Rev. Lett. **116**, 061102 (2016).

[2] LIGO Scientific Collaboration and Virgo Collaboration, Phys. Rev. Lett. **119**, 161101 (2017).

[3] LIGO Scientific Collaboration, Virgo Collaboration, *et al.*, Astrophys. J. Lett. **848**, 2 (2017).

[4] C. Everitt *et al.*, Class. Quantum Grav. **25**, 11 (2008).

[5] P. Touboul *et al.*, Phys. Rev. Lett. **119**, 231101 (2017).

[6] C. M. Will, Living Rev. Relativity **17**, 4 (2014).

[7] KAGRA Collaboration, Progr. Theor. Exp. Phys. **2018**, 013F01 (2018).

[8] IndIGO Consortium, "LIGO-India: Proposal for an interferometric gravitational-wave observatory," (2011).

[9] ET Science Team, ET-0106C-10 **4** (2011).

[10] M. Armano *et al.*, Phys. Rev. Lett. **120**, 061101 (2018).

[11] LISA Consortium, "LISA: A proposal in response to the ESA call for L3 mission concepts," arXiv:1702.00786 .

[12] S. Kawamura *et al.*, Class. Quantum Grav. **23**, 0264 (2006).

[13] K. Yagi and N. Seto, Phy. Rev. D **83**, 044011 (2011).

[14] S. Isoyama, H. Nakano, and T. Nakamura, "Multiband Gravitational-Wave Astronomy: Observing binary inspirals with a decihertz detector, B-DECIGO," arXiv:1802.06977v1 .

[15] A. Nishizawa, A. Taruya, K. Hayama, S. Kawamura, and S. Masa-aki, Phys. Rev. D **79**, 082002 (2009).

[16] A. Nishizawa, A. Taruya, and S. Kawamura, Phys. Rev. D **81**, 104043 (2010).

[17] B. Allen and J. D. Romano, Phys. Rev. D **59**, 102001 (1999).

[18] M. Maggiore, *Gravitational Waves*, Vol. 1: Theory and Experiments (Oxford University Press, 2008).

[19] The LIGO Scientific Collaboration, Class. Quantum Grav. **32**, 074001 (2015).

[20] D. V. Martynov *et al.*, Phys. Rev. D **93**, 112004 (2016).